The Electrochemistry of Charge Injection at the Electrode/Tissue Interface

Daniel R. Merrill

Abstract The physical basis for electrical stimulation of excitable tissue is presented with emphasis on the fundamental mechanisms of charge injection at the electrode/tissue interface. Faradaic and non-Faradaic charge-transfer mechanisms are presented and contrasted. An electrical model of the electrode/tissue interface is given. The physical basis for the origin of electrode potentials is given. Electrochemical reversibility is discussed. Two-electrode and three-electrode systems are compared. Various methods of controlling charge delivery during pulsing are presented. Commonly used electrode materials and stimulation protocols are reviewed in terms of stimulation efficacy and safety. Principles of stimulation of excitable tissue are reviewed. Mechanisms of damage to tissue and the electrode are reviewed.

Contents

D.R. Merrill (✉)
Alfred E. Mann Foundation for Scientific Research, Santa Clarita, CA 91355, USA
e-mail: danm@aemf.org

This chapter is adapted from a previously published review [1].

D.D. Zhou, E. Greenbaum (eds.), *Implantable Neural Prostheses 2*,
Biological and Medical Physics, Biomedical Engineering, DOI 10.1007/978-0-387-98120-8_4,

1 Physical Basis of the Electrode/Electrolyte Interface

Electrical stimulation of excitable tissue is the basis of clinical therapeutic electrical stimulation and functional electrical stimulation, including deep brain stimulation and stimulation of muscles, peripheral nerves, or sensory systems. When a metal electrode is placed inside a physiological medium such as extracellular fluid (ECF), an interface is formed between the two phases. In the metal electrode phase and in attached electrical circuits, charge is carried by electrons. In the physiological medium, or in more general electrochemical terms the electrolyte, charge is carried by ions, including sodium, potassium, and chloride in the ECF. The central process that occurs at the electrode/electrolyte interface is a transduction of charge carriers from electrons in the metal electrode to ions in the electrolyte.

In the simplest system, two electrodes are placed in an electrolyte, and electrical current may pass between the electrodes through the electrolyte. One of the two electrodes is termed a working electrode (WE), and the second is termed a counter electrode (CE). The working electrode is defined as the electrode that one is interested in studying, with the counter electrode being necessary to complete the circuit for charge conduction. In electrophysiology experiments, it is common to use a third electrode termed the reference electrode (RE), which defines a reference for electrical potential measurements.

A change in electrical potential occurs upon crossing from one conducting phase to another (from the metal electrode to the electrolyte) at the interface itself, in a very narrow interphase region (at most a few hundred angstroms in width). The basis for this is described in more detail in Section 1.4. The change or gradient in electrical potential corresponds to an electric field, measured in volts/meter, at the interface. This gradient exists even in the equilibrium condition when there is no current flow. Electrochemical reactions may occur in this interphase region if the electrical potential profile is forced away from the equilibrium condition. In the absence of current, the electrical potential is constant throughout the electrolyte beyond the narrow interphase region. During current flow, a potential gradient exists in the electrolyte, generally many orders of magnitude smaller than at the interface.

There are two primary mechanisms of charge transfer at the electrode-electrolyte interface, illustrated in Fig. 1. One is a non-Faradaic reaction, where no electrons are

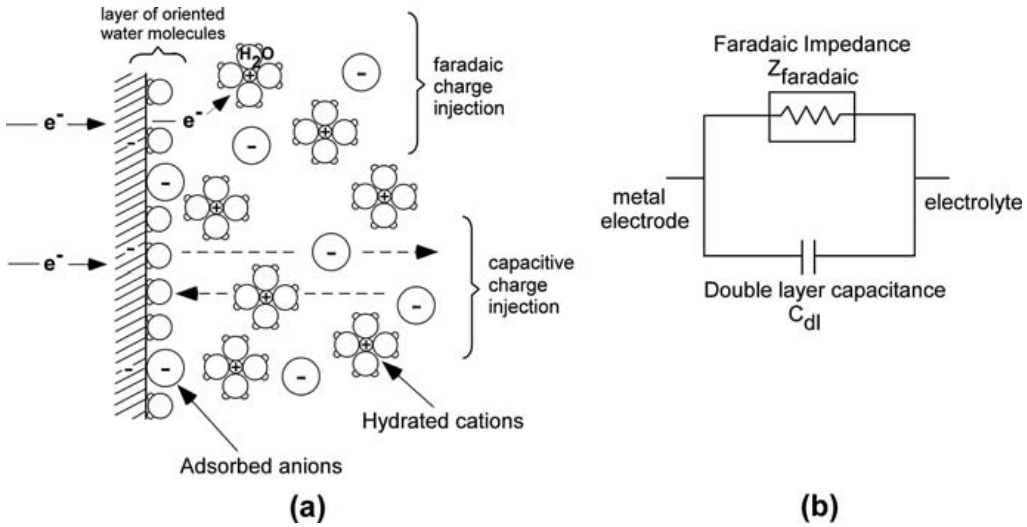

Fig. 1 The electrode/electrolyte interface, illustrating Faradaic charge transfer (*top*) and capacitive redistribution of charge (*bottom*) as the electrode is driven negative. (**a**) Physical representation (**b**) Two-element electrical circuit model for mechanisms of charge transfer at the interface. The capacitive process involves reversible redistribution of charge. The Faradaic process involves transfer of electrons from the metal electrode, reducing hydrated cations in solution (symbolically $O + e^- \rightarrow R$, where the cation O is the oxidized form of the redox couple O/R). An example reaction is the reduction of silver ions in solution to form a silver plating on the electrode, reaction (8a). Faradaic charge injection may or may not be reversible

transferred between the electrode and electrolyte. Non-Faradaic reactions include redistribution of charged chemical species in the electrolyte. The second mechanism is a Faradaic reaction in which electrons are transferred between the electrode and electrolyte, resulting in reduction or oxidation of chemical species in the electrolyte. Faradaic reactions are further divided into reversible and nonreversible Faradaic reactions, which are detailed in Section 1.3. Reversible Faradaic reactions include those where the products either remain bound to the electrode surface or do not diffuse far away from the electrode. In an irreversible Faradaic reaction, the products diffuse away from the electrode.

1.1 Capacitive/Non-Faradaic Charge Transfer

If only non-Faradaic redistribution of charge occurs, the electrode/electrolyte interface may be modeled as a simple electrical capacitor called the double-layer capacitor C_{dl}. This capacitor is formed due to several physical phenomena [2, 3, 4, 5, 6]. First, when a metal electrode is placed in an electrolyte, charge redistribution occurs as metal ions in the electrolyte combine with the electrode. This involves a transient transfer of electrons between the two phases, resulting in a plane of charge at the surface of the metal electrode, opposed by a plane of opposite charge, as counterions, in the electrolyte. The excess charge on the electrode surface, symbolized

by q^M or σ^M, takes the form of an excess or deficiency of electrons and is present on a very thin layer (< 0.1 angstrom thick) at the surface. In the electrolyte, counterions take the form of excess cations or anions, symbolized by q^S. If q^M is an excess of electrons, then q^S is an excess of cations, and if q^M is a deficiency of electrons, then q^S is an excess of anions, i.e., net electroneutrality is maintained and $q^M = -q^S$. A second reason for formation of the double layer is that some chemical species such as halide anions may specifically adsorb to the solid electrode, acting to separate charge. A third reason is that polar molecules such as water may have a preferential orientation at the interface, and the net orientation of polar molecules separates charge.

If the net charge on the metal electrode is forced to vary (as occurs with charge injection during stimulation), a redistribution of charge occurs in the solution. Consider two metal electrodes immersed in an electrolytic salt solution. A voltage source is applied across the two electrodes so that one electrode is driven to a relatively negative potential and the other to a relatively positive potential. At the interface that is driven negative, the metal electrode has an excess of negative charge (Fig. 1). This will attract positive charge (cations) in solution toward the electrode and repel negative charge (anions). In the interfacial region, there will be net electroneutrality, because the negative charge excess on the electrode surface will equal the positive charge in solution near the interface. The bulk solution will also have net electroneutrality. At the second electrode, the opposite processes occur, i.e., the repulsion of anions by the negative electrode is countered by attraction of anions at the positive electrode. If the total amount of charge delivered is sufficiently small, only charge redistribution occurs, there is no transfer of electrons across the interface, and the interface is well modeled as a simple capacitor. *If the polarity of the applied voltage source is then reversed, the direction of current is reversed, the charge redistribution is reversed, and charge that was injected from the electrode into the electrolyte and stored by the capacitor may be recovered.*

1.2 Faradaic Charge Transfer and the Electrical Model of the Electrode/Electrolyte Interface

Charge may also be injected from the electrode to the electrolyte by Faradaic processes of reduction and oxidation, whereby electrons are transferred between the two phases. Reduction, which requires the addition of an electron, occurs at the electrode that is driven negative, while oxidation, requiring the removal of an electron, occurs at the electrode that is driven positive. Faradaic charge injection results in the creation of chemical species, which may either go into the solution or remain bound to the electrode surface. Unlike the capacitive charge injection mechanism, if these Faradaic reaction products diffuse sufficiently far away from the electrode, they cannot be recovered upon reversing the direction of current. Fig. 1(b) illustrates a simple electrical circuit model of the electrode/electrolyte interface consisting of two elements [7, 8, 9]. C_{dl} is the double-layer capacitance representing the ability

of the electrode to cause charge flow in the electrolyte without electron transfer. Z_{faradaic} is the Faradaic impedance representing the Faradaic processes of reduction and oxidation where electron transfer occurs between the electrode and electrolyte. One may generally think of the capacitance as representing charge storage, and the Faradaic impedance as representing charge dissipation.

The following are illustrative examples of Faradaic electrode reactions that may occur. Cathodic processes, defined as those where reduction of species in the electrolyte occur as electrons are transferred from the electrode to the electrolyte, include such reactions as

$$2\,H_2O + 2e^- \rightarrow H_2 \uparrow 2\,OH^- \quad \text{reduction of water} \tag{1}$$

$$Fe^{3+} + e^- \longleftrightarrow Fe^{2+} \quad \text{simple electron transfer} \tag{2}$$

$$Cu^{2+} + 2\,e^- \longleftrightarrow Cu \quad \text{metal deposition} \tag{3}$$

$$PtO + 2H^+ + 2e^- \longleftrightarrow Pt + H_2O \quad \text{oxide formation and reduction} \tag{4}$$

$$IrO + 2H^+ + 2\,e^- \longleftrightarrow Ir + H_2O \quad \text{oxide formation and reduction} \tag{5a}$$

$$IrO_2 + 4H^+ + 4\,e^- \longleftrightarrow Ir + 2H_2O \quad \text{oxide formation and reduction} \tag{5b}$$

$$2IrO_2 + 2H^+ + 2\,e^- \longleftrightarrow Ir_2O_3 + H_2O \quad \text{oxide formation and reduction} \tag{5c}$$

$$Pt + H^+ + e^- \longleftrightarrow Pt - H \quad \text{hydrogen atom plating} \tag{6}$$

$$M^{(n+1)+}\,(OH)_{(n+1)} + H^+ + e^- \longleftrightarrow M^{n+}\,(OH)_n + H_2O \quad \text{valency changes within an oxide} \tag{7}$$

$$Ag^+ + e^- \longleftrightarrow Ag \quad \text{reduction of silver ions} \tag{8a}$$

$$AgCl \longleftrightarrow Ag^+ + Cl^- \quad \text{dissolution of silver chloride} \tag{8b}$$

Anodic processes, defined as those where oxidation of species in the electrolyte occur as electrons are transferred to the electrode, include:

$$2H_2O \rightarrow O_2 \uparrow + 4\,H^+ + 4\,e^- \quad \text{oxidation of water} \tag{9}$$

$$Pt + 4Cl^- \rightarrow [PtCl_4]^{2-} + 2\,e^- \quad \text{corrosion} \tag{10}$$

$$2Cl^- \rightarrow Cl_2 \uparrow + 2\,e^- \quad \text{gas evolution} \tag{11}$$

$$\mathrm{Fe} \rightarrow \mathrm{Fe}^{2+} + 2\,e^{-} \qquad \text{anodic dissolution} \tag{12}$$

$$2\,\mathrm{Ag} + 2\mathrm{OH}^{-} \longleftrightarrow \mathrm{Ag_2O} + \mathrm{H_2O} + 2\,e^{-} \qquad \text{oxide formation} \tag{13}$$

Reaction (1) is the irreversible reduction of water (which is typically abundant as a solvent at 55.5 M) forming hydrogen gas and hydroxyl ions. The formation of hydroxyl raises the pH of the solution. Reversible reactions, where species remain bound or close to the electrode surface, are demonstrated by reactions (2), (3), (4), (5), (6), (7), and (8). In reaction (2), the electrolyte consists of ferric and ferrous ions. By driving the metal electrode to more negative potentials, electrons are transferred to the ferric ions forming ferrous ions. In reaction (3) a copper metal electrode is immersed in a solution of cuprous ions. The cuprous ions in the solution are reduced, building up the copper electrode. Reactions (4) and (5a), (5b), (5c) are the reversible formation and subsequent reduction of an oxide layer on platinum and iridium, respectively. Reaction (6) is reversible adsorption of hydrogen onto a platinum surface responsible for the so-called pseudocapacity of platinum. Reaction (7) is the general form of reversible valency changes that occur in a multilayer oxide film of iridium, ruthenium, or rhodium, with associated proton or hydroxyl ion transfer [10, 11, 12, 13]. Reactions (8a) and (8b) are the reversible reactions of a silver chloride electrode driven cathodically. Silver ions in solution are reduced to solid silver on the electrode (reaction 8a). To maintain the solubility constant $K_S \equiv (a_{Ag+})(a_{Cl-})$, where a is the ionic activity, as silver ions in solution are reduced the AgCl salt covering the electrode dissolves to form silver and chloride ions in solution (reaction 8b) (these reactions are discussed in more detail at the end of this section). In reaction (9), water molecules are irreversibly oxidized forming oxygen gas and hydrogen ions, and thus lowering the pH. Reaction (10) is the corrosion of a platinum electrode in a chloride-containing media. In reaction (11), chloride ions in solution are oxidized forming chlorine gas. In reaction (12), an iron metal electrode is dissolved forming ferrous ions that go into solution. Reaction (13) represents a reversible oxide formation on a silver electrode. As electrons are removed from the silver metal, Ag^+ ions are formed. These Ag^+ ions then combine with hydroxyl (OH^-) ions from solution forming an oxide layer (Ag_2O) on the surface of the silver electrode. Note the transfer of charge that occurs. As electrons are transferred to the electrode and then the external electrical circuit, the silver electrode is oxidized ($Ag \rightarrow Ag^+$). Because hydroxyl ions associate with the silver ions, the silver oxide is electroneutral. However, since hydroxyl has been removed from the solution, there is a net movement of negative charge from the electrolyte (loss of hydroxyl) to the electrode (electrons transferred to the electrode and then to the electrical circuit). The loss of hydroxyl lowers the solution pH.

1.3 Reversible and Irreversible Faradaic Reactions

There are two limiting cases that may define the net rate of a Faradaic reaction [9, 14, 15]. At one extreme, the reaction rate is under kinetic control; at the other extreme, the reaction rate is under mass transport control. For a given metal electrode and

electrolyte, there is an electrical potential (voltage) called the equilibrium potential where no net current passes between the two phases. At electrical potentials sufficiently close to equilibrium, the reaction rate is under kinetic control. Under kinetic control, the rate of electron transfer at the interface is determined by the electrode potential and is *not* limited by the rate at which reactant is delivered to the electrode surface (the reaction site). When the electrode potential is sufficiently different from equilibrium, the reaction rate is under mass transport control. In this case, all reactant that is delivered to the surface reacts immediately, and the reaction rate is limited by the rate of delivery of reactant to the electrode surface.

Faradaic reactions are divided into reversible and irreversible reactions [9]. The degree of reversibility depends on the relative rates of kinetics (electron transfer at the interface) and mass transport. A Faradaic reaction with very fast kinetics relative to the rate of mass transport is reversible. With fast kinetics, large currents occur with small potential excursions away from equilibrium. Since the electrochemical product does not move away from the surface extremely fast (relative to the kinetic rate), there is an effective storage of charge near the electrode surface, and *if the direction of current is reversed then some product that has been recently formed may be reversed back into its initial (reactant) form.*

FAST KINETICS RELATIVE TO MASS TRANSPORT →
CHARGE - STORAGE CAPACITY = REVERSIBLE

In a Faradaic reaction with slow kinetics, large potential excursions away from equilibrium are required for significant currents to flow. In such a reaction, the potential must be forced very far from equilibrium before the mass transport rate limits the net reaction rate. In the lengthy time frame imposed by the slow electron-transfer kinetics, chemical reactant is able to diffuse to the surface to support the kinetic rate, and product diffuses away quickly relative to the kinetic rate. Because the product diffuses away, there is no effective storage of charge near the electrode surface, in contrast to reversible reactions. *If the direction of current is reversed, product will not be reversed back into its initial (reactant) form, since it has diffused away within the slow time frame of the reaction kinetics*. Irreversible products may include species that are soluble in the electrolyte (e.g., reaction 12), precipitate in the electrolyte, or evolve as a gas (e.g., reactions 1, 9, and 11). Irreversible Faradaic reactions result in a net change in the chemical environment, potentially creating chemical species that are damaging to tissue or the electrode. Thus, as a general principle, an objective of electrical stimulation design is to avoid irreversible Faradaic reactions.

SLOW KINETICS → NO CHARGE - STORAGE CAPACITY
(PRODUCT DIFFUSES AWAY) = IRREVERSIBLE

In certain Faradaic reactions, the product remains bound to the electrode surface. Examples include hydrogen atom plating on platinum (reaction 6) and oxide formation (reaction 13 as an example). These can be considered a logical extreme of slow

mass transport. Since the product remains next to the electrode, such reactions are a basis for reversible charge injection.

1.4 The Origin of Electrode Potentials and the Three-Electrode Electrical Model

Electrochemical potential is a parameter that defines the driving force for all chemical processes and is the sum of a chemical potential term and an electrical potential term [16]. It is defined as

$$\overline{\mu}_i^{\beta} \equiv \mu_i^{\beta} + z_i\, e\, \phi^{\beta} \tag{14}$$

where $\overline{\mu}_{\mathrm{i}}^{\beta}$is the electrochemical potential of particle i in phase β, $\mu_{\mathrm{i}}{}^{\beta}$is the chemical potential of particle i in phase β, and ϕ^{β} is the inner potential of the particle in phase β (the electrical potential in the bulk).

Two phases in contact are defined to be in electrochemical equilibrium when the electrochemical potential of any given chemical species is the same in each phase. If the electrochemical potentials of some species are unequal, there is a driving force for the net transfer of such species between the phases. For a metal electrode and a solution of metal ions in contact to be in equilibrium, the electrochemical potential of an electron must be the same in each phase. When two isolated phases are brought into contact, electron transfer may occur if the electrochemical potentials are unequal. Consider immersing a metal electrode into an electrolyte with an electrochemical reduction/oxidation (redox) couple, for example ferric and ferrous ions ($Fe^{3+}$and Fe^{2+}). Assume that while in isolation, the metal electrode has a higher chemical potential for electrons than the redox couple. Upon bringing the electrode into contact with the electrolyte, electrons will transfer from the metal to the redox couple, driving the reaction $Fe^{3+} + e^{-} \rightarrow Fe^{2+}$ to the right as ferric ions are reduced to ferrous ions. Upon transferring electrons, an electrical potential difference develops between the phases that repels further transfer. Equilibrium is reached when the electrostatic force cancels the driving force due to a difference in chemical potentials for an electron. At equilibrium, there is no further transfer of electrons, and a distinctive difference in inner potentials $\Delta\phi$ exists between the two phases (the inner potential ϕ is the electrical potential inside the bulk of the phase). The difference in inner potentials between a metal phase and solution phase in contact, $\Delta\phi_{\text{metal - solution}}$, defines the electrode interfacial potential.

It is an experimental limitation that a single interfacial potential cannot be measured. Whenever a measuring instrument is introduced, a new interface is created, and one is unable to separate the effects of the two interfaces. It is tempting to wonder why one cannot simply place one voltmeter probe on a metal electrode and a second voltmeter probe into the electrolyte and measure an electrode potential, as shown in Fig. 2. The electrode potential of interest is $\Delta\phi_{\text{metal - solution}}$. By introducing the measuring device (a metal voltmeter probe) into the electrolyte solution, a new interface is created with its own

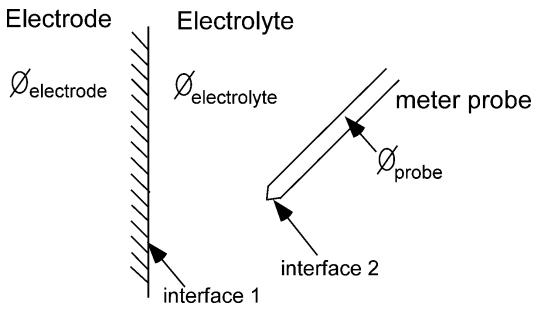

Fig. 2 Voltmeter Probe in an Electrolyte Introduction of the metal probe creates a second electrode/electrolyte interface

difference in potentials $\Delta\phi_{\text{solution - probe}}$. It is impossible to separate the components $\Delta\phi_{\text{metal - solution}}$ and $\Delta\phi_{\text{solution - probe}}$ from the measured potential. Note that if the other voltmeter probe (touching the metal electrode, not shown in Fig. 2) consists of a different material than the electrode, a third interface is formed, with a third difference in inner potentials.

Evaluation must be of a complete electrochemical cell, which is generally considered as two electrodes separated by an electrolyte. Practically, potentials are measured as complete cell potentials between two electrodes, either from the working electrode to the counter electrode or from the working electrode to a reference electrode. A cell potential is the sum of two interfacial potentials (electrode$_1$ to electrolyte plus electrolyte to electrode$_2$), as well as any potential difference occurring across the electrolyte as current flows. In the absence of current, the cell potential between the working electrode and second (counter or reference) electrode is called the open-circuit potential and is the sum of two equilibrium interfacial potentials from the working electrode to the electrolyte and from the electrolyte to the second electrode.

The term "electrode potential" is not defined consistently in the electrochemistry literature. Some authors define the electrode potential as the potential between an electrode and a reference electrode, and others define it as the (immeasurable) interfacial potential. For clarity and accuracy, when the term "electrode potential" is used it should be specified what this potential is with respect to, e.g., the electrolyte, a reference electrode, or another electrode.

Consider the electron-transfer reaction between a metal electrode and a reduction/oxidation (redox) couple O and R in solution:

$$\mathrm{O} + n\,e^- \longleftrightarrow \mathrm{R} \tag{15}$$

where O is the oxidized species of the couple, R is the reduced species, and n is the number of electrons transferred

If the concentrations of both O and R in solution are equal, then the electrical potential of the redox couple equilibrates at $E^{\Theta'}$, defined as the formal potential. More generally, if the concentrations of O and R are unequal, the equilibrium potential or Nernst potential, E_{eq}, may be calculated by the Nernst equation [9,16]:

$$E_{\text{eq}} = E^{\Theta\prime} + (RT/nF)\ln\{[\mathrm{O}]\,/\,[\mathrm{R}]\} \tag{16}$$

where [O] and [R] are concentrations in the bulk solution, R is the gas constant $\sim$ 8.314 J/mol-$^{\circ}$K, T is the absolute temperature, and F is Faraday's constant $\sim$96,485 C/mol of electrons

The Nernst equation (16) relates the equilibrium electrode potential E_{eq} (the electrical potential of the working electrode with respect to any convenient reference electrode) to the bulk solution concentrations [O] and [R] when the system is in equilibrium. As the bulk concentration [O] increases or the bulk concentration [R] decreases, the equilibrium potential becomes more positive.

In a system containing only one redox couple that has fairly fast kinetics, the measured open-circuit potential equals the equilibrium potential of the redox couple. If the kinetics of the redox couple are slow, the open-circuit potential (an empirical parameter) may not quickly attain the equilibrium potential after a perturbation, and if other contaminating redox couples (affectionately known as "dirt") are present that affect the equilibrium state, the measured open-circuit potential does not readily correlate with any single redox equilibrium potential.

If one begins with a system that is in equilibrium and then forces the potential of an electrode away from its equilibrium value, for example by connecting a current source between the working and counter electrodes, the electrode is said to become polarized. Polarization is measured by the overpotential η, which is the difference between an electrode's potential and its equilibrium potential (both measured with respect to some reference electrode):

$$\eta \equiv E - E_{eq} \tag{17}$$

The electrode interface model of Fig. 1(b) demonstrates the mechanisms of charge injection from an electrode; however, it neglects the equilibrium interfacial potential $\Delta\phi$ that exists across the interface at equilibrium. This is modeled as shown in Fig. 3(a). In addition to the electrode interface, the solution resistance R_S (alternatively referred to as the access resistance R_A or the ohmic resistance R_Ω) that exists between two electrodes in solution is modeled.

An electrical potential difference, or voltage, is always defined between two points in space. During electrical stimulation, the potentials of both the working and counter electrodes may vary with respect to some third reference point. A third electrode whose potential does not change over time, the reference electrode, may be employed for making potential measurements. Potentials of the working electrode and counter electrode may then be given with respect to the reference electrode. An electrical circuit model of a three-electrode system, including the working electrode, counter electrode, and reference electrode immersed into an electrolyte, is shown in Fig. 3(b). The reference electrode is used for potential measurements and is not required to pass current for stimulation; a two-electrode system (working and counter electrodes) is sufficient for stimulation. As current is passed between the working and counter electrodes through the electrolytic solution, the interfacial potentials, $V_{WE\text{-}solution}$ and $V_{CE\text{-}solution}$, will vary from their equilibrium values, i.e., there are overpotentials associated with both interfaces. Also, as current flows there is a voltage drop across the resistive solution equal to the product of current

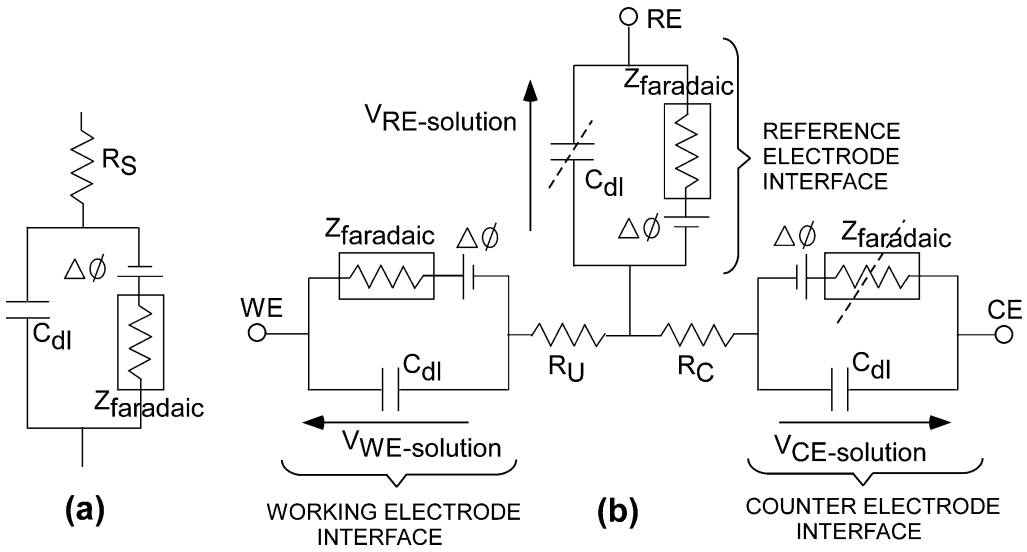

Fig. 3 Electrical Circuit Models (a) Single-Electrode/Electrolyte Interface (b) Three-Electrode System External access to the system is at three points labeled "WE", "CE", and "RE". If the counter electrode has a large surface area, it may be considered as strictly a capacitance as shown. A reference electrode with very low valued Faradaic resistance will maintain the interfacial potential $V_{\text{RE-solution}}$ constant

and solution resistance: $v = iR_S$. Thus, if current flows and there is a change in the measured potential $V_{\text{WE-CE}}$, this change may be from any of three sources: (1) an overpotential at the working electrode as the interfacial potential $V_{\text{WE-solution}}$ varies, (2) an overpotential at the counter electrode as the interfacial potential $V_{\text{CE-solution}}$ varies, and (3) the voltage drop iR_S in solution. In the two-electrode system, one may only measure $V_{\text{WE-CE}}$, and the individual components of the two overpotentials and iR_S cannot be resolved. A third (reference) electrode may be used for potential measurements. An ideal reference electrode has a Faradaic reaction with very fast kinetics, which appears in the electrical model as a very low resistance for the Faradaic impedance Z_{faradaic}. In this case, no significant overpotential occurs at the reference electrode during current flow, and the interfacial potential $V_{\text{RE-solution}}$is considered constant. Examples of common reference electrodes are the reversible hydrogen electrode (RHE), the saturated calomel electrode (SCE), and the silver-silver chloride electrode [17]. In the three-electrode system, if current flows through the working and counter electrodes and a change is noted in the measured potential $V_{\text{WE-RE}}$, this change may be from either of two sources: (1) an overpotential at the working electrode as the interfacial potential $V_{\text{WE-solution}}$ varies, and (2) the voltage drop iR_S in solution. Unlike the two-electrode system, only one overpotential contributes to the measured potential change. Furthermore, the overpotential at the working electrode can be estimated using the process of correction. This involves estimating the value of the solution resistance between the working electrode interface and the reference electrode interface, called the uncorrected solution resistance R_U, and multiplying R_U by the measured current. This product $V_{\text{corr}} = iR_{\text{U estimated}}$ is then subtracted from the measured $V_{\text{WE-RE}}$ to yield the two interfacial

potentials $V_{\text{WE-solution}}$ and $V_{\text{RE-solution}}$. Since $V_{\text{RE-solution}}$ is constant, any change in $V_{\text{WE-RE}}$ is attributed to an overpotential at the working electrode interface. Figure 4 illustrates the electrical potential profiles of a two-electrode system and a three-electrode system, under conditions of no current flow and with current.

1.5 Faradaic Processes: Quantitative Description

Equation (18) below, the current–overpotential equation [9], relates the overpotential to net current density through an electrode going into a Faradaic reaction and defines the full characteristics of the Faradaic impedance.

$$i_{\text{net}} = i_0\{\frac{[\text{O}]\,(0,t)}{[\text{O}]_\infty}\exp\left(-\alpha_c n f\,\eta\right) - \frac{[\text{R}]\,(0,t)}{[\text{R}]_\infty}\exp\left(+\,(1-\alpha_c)\,n f \eta\right)\} \qquad (18)$$

where i_{net} is the net Faradaic current density across the electrode/electrolyte interface, i_0 is the exchange current density, [O](0,*t*) and [R](0,*t*) are concentrations at the electrode surface ($x = 0$) as a function of time, $[\text{O}]_\infty$ and $[\text{R}]_\infty$ are bulk concentrations, $\alpha_c$is the cathodic transfer coefficient and equals ~0.5, n is the number of moles of electrons per mole of reactant oxidized (equation 15), $f \equiv F/R\,T$, F is Faraday's constant ~96,485 C/mol of electrons, R is the gas constant ~ 8.314 J/mol-°K, and T is the absolute temperature

This equation relates the net current of a Faradaic reaction to three factors of interest: (1) the exchange current density i_0, which is a measure of the kinetic rate of the reaction, (2) an exponential function of the overpotential, and (3) the concentration of reactant at the electrode interface. The exponential dependence of Faradaic current on overpotential indicates that for a sufficiently small overpotential, there is little Faradaic current, i.e., for small potential excursions away from equilibrium, current flows primarily through the capacitive branch of Fig. 1, charging the electrode capacitance, not through the Faradaic branch. As more charge is delivered through an electrode interface, the electrode capacitance continues to charge, the overpotential increases, and the Faradaic current (proportional to exp (η)) begins to be a significant fraction of the total injected current. For substantial cathodic overpotentials, the left term of equation (18) dominates; for substantial anodic overpotentials, the right term dominates.

The two exponential terms represent the reduction and oxidation rates, respectively. The net current is the sum of the reduction and oxidation currents, as shown in Fig. 5. At the equilibrium potential E_{eq}, when $\eta = 0$, the rates are equal and opposite and may be relatively small (compared to when driven away from equilibrium), and the net current is zero. As the electrode potential moves away from equilibrium, one or the other term will begin to dominate. At overpotentials near equilibrium, the current increases rapidly with changes in overpotential due to the exponential form of equation (18).

A large value for i_0 represents a reaction with rapid electron exchange between the electrode and electrolyte (called the heterogeneous reaction); a small value for i_0 represents a reaction with slow electron transfer in the heterogeneous reaction. The

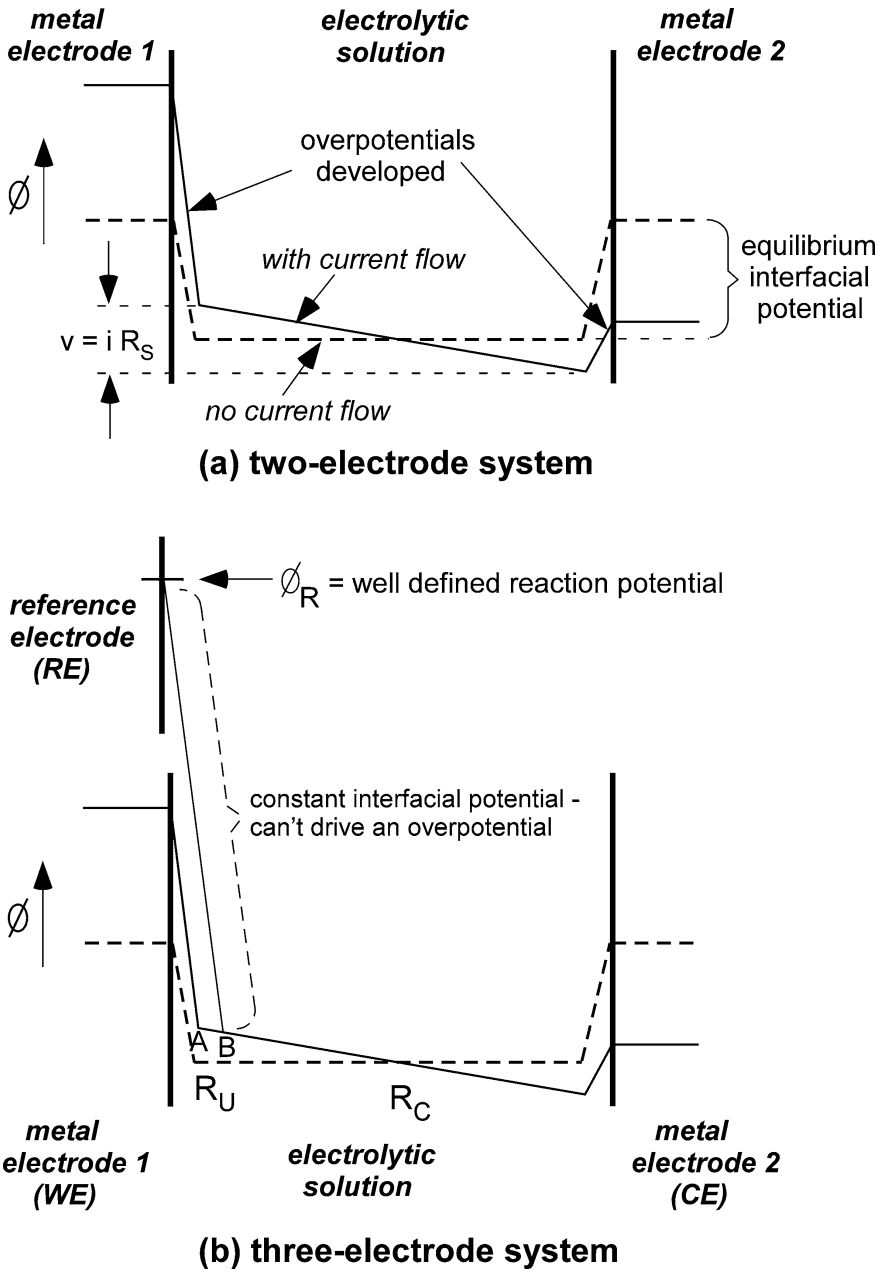

Fig. 4 Electrical Potential Profiles (**a**) Two-electrode system. In the absence of current, two equilibrium interfacial potentials exist, and the cell potential measured between the two electrodes is the difference between these equilibrium potentials. As shown the equilibrium potentials are the same (as would be the case if the same metal was used for both electrodes), and the cell potential would be zero. Upon passing current, overpotentials develop at both interfaces (one interfacial potential becomes greater, one smaller). The net change in measured cell potential is due to three sources: the voltage drop in solution $i\,R_S$ and two overpotentials η_1 and η_2. (**b**) Three-electrode system. The measured potential is between the working electrode and reference electrode. Since no substantial overpotential can be developed at the reference electrode, any change in measured potential upon passing current is due to two sources: the overpotential at the working electrode-solution interface, and the solution drop $i\,R_U$, where the uncorrected resistance R_U is the solution resistance between the WE interface and RE interface

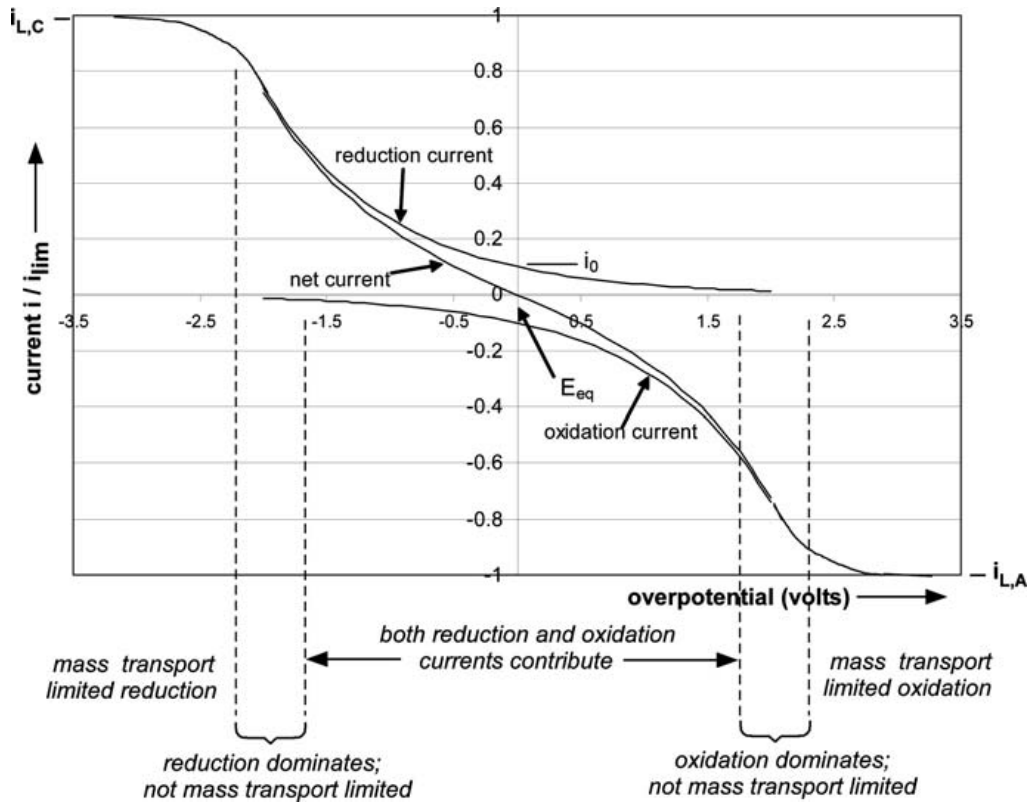

Fig. 5 Net Current vs. Overpotential, Oxidation and Reduction Curves Three characteristic regions are displayed: (1) near equilibrium, both reduction and oxidation currents contribute, then as the overpotential increases, (2) either reduction or oxidation dominate, initially in the absence of mass-transport limitation, and then (3) with mass-transport limitation

values for exchange current density i_0 may range over several orders of magnitude, e.g., from 10^{+1} to 10^{-12}A/cm^2. In the example shown in Fig. 5, i_0 is 0.1 of i_L, the limiting current. Figure 6 illustrates how the current–overpotential relation is highly dependent upon the exchange current. Three values of exchange current density are plotted. In each case $\alpha_c = 0.5$, so the plot is symmetric about $\eta = 0$. For a kinetically fast system with a large exchange current density, such as $i_0 = 10^{-3}$A/cm^2, no significant overpotential may be achieved before a large current ensues. As the exchange current density decreases, one must go to higher overpotentials (further from the equilibrium value of $\eta = 0$) before a given current is noted. For a finite detection level of current (a real instrument), a reaction with low exchange current density will not manifest until relatively high overpotentials are achieved.

If currents are low or if the electrolytic solution is well stirred, so that the surface concentrations [O](0,t) and [R](0,t) are essentially equal to the bulk concentrations, then equation (18) reduces to

$$i_{\text{net}} = i_0 \{\exp\ (-\alpha_c\, nf\, \eta) - \exp\,(+\,(1-\alpha_c)\ \ nf\, \eta)\} \tag{19}$$

This is the Butler-Volmer equation, which describes the current–overpotential relationship when mass-transfer effects are negligible. This may be a useful approximation of (18) when the current is less than 10% of the limiting current.

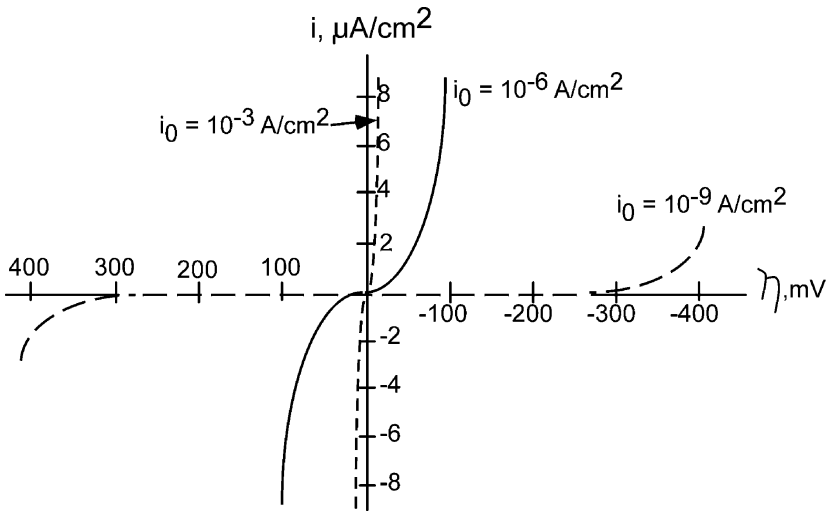

Fig. 6 Current–Overpotential Dependence on Exchange Current Density Three example exchange current densities are shown. Large densities correspond to kinetically fast reactions. At large exchange current densities, little overpotential is required for substantial current density

As η increases away from zero, one of the two terms of the current–overpotential relationship (representing either reduction or oxidation) will dominate:

$$\text{for negative overpotentilas} \qquad i_{net} = i_0 \exp\left(-\alpha_c\, nf\, \eta\right) \tag{20a}$$

$$\text{for positive overpotentials} \qquad i_{\text{net}} = i_0 \left\{-\exp\left(+\left(1-\alpha_c\right)\, nf\, \eta\right)\right\} \tag{20b}$$

Near equilibrium, the surface concentrations of O and R are approximately equal to the bulk concentrations. As more charge is delivered and the overpotential continues to increase (in either direction), the surface concentration of reactant may decrease. The Faradaic current will then begin to level off, corresponding to the current becoming limited by mass transport of reactant, not electron transfer kinetics. At the limiting currents, $i_{\text{L,c}}$(cathodic, for negative overpotentials) or $i_{\text{L,a}}$(anodic, for positive overpotentials), the reactant concentration at the electrode surface approaches zero, and the terms $[\text{O}](0,t)/[\text{O}]_\infty$ or $[\text{R}](0,t)/[\text{R}]_\infty$ counteract the exponential terms in equation (18), dominating the solution for net reaction rate. At the limiting currents, the slope of the reactant concentration gradient between the electrode surface and the bulk electrolyte determines the rate of reactant delivery, and thus the current. At overpotentials where mass transport limitation effects occur (but prior to $i_{\text{L,c}}$ or $i_{\text{L,a}}$), Faradaic current takes the form:

$$\text{for negative overpotentials} i_{\text{net}} = \frac{[\text{O}]\,[0,t]}{[\text{O}]_\infty} i_0 \exp\left(-\alpha_c\, nf\, \eta\right) \tag{21a}$$

$$\text{for positve overpotentials} i_{\text{net}} = -\frac{[\text{R}]\,[0.t]}{R_\infty} i_0 \exp\left(+\left(1-\alpha_c\right)\, nf\, \eta\right) \tag{21b}$$

Equations (19), (20), and (21) are illustrated as three regions on the current–overpotential plot, shown in Fig. 5.

The mass transport limited currents $i_{L,c}$ and $i_{L,a}$ are given by equations (22a) and (22b) below.

$$i_{L,c} = -n\,F\,A\,k_{d,O}\,[O]_\infty \tag{22a}$$

$$i_{L,a} = n\,F\,A\,k_{d,R}\,[R]_\infty \tag{22b}$$

where A is the electrode area and k_d is the mass transport rate, given by $k_d = D/\delta$, where D is the diffusion coefficient and δ is the diffusion layer thickness

For very small overpotentials, the Butler-Volmer equation (19) can be approximated by

$$i_{net} = i_0\,(-nf\,\eta) \tag{23}$$

since $e^x \sim 1 + x$ for small x. Thus at small overpotentials, the current is a linear function of overpotential. The ratio $-\,\eta\,/i$ is called the charge transfer resistance R_{ct}, which is given by

$$R_{ct} = R\,T/n\,F\,i_0 \tag{24}$$

A small value for R_{ct} corresponds to a kinetically fast reaction.

When the overpotential is relatively large, only one of the two terms in (18) is significant, and either the reduction current or the oxidation current becomes negligible. Figure 7 is a Tafel plot, which is a plot of log i vs. η. The straight-line approximations of Fig. 7, with slopes of $-\,\alpha\,n\,F/2.3\,R\,T$ for the cathodic reaction and $(1-\alpha)\,n\,F/2.3\,R\,T$ for the anodic reaction, are good approximations when the reverse reaction supplies less than 1% of the total current. Note that the intercept of the straight lines on the $\eta = 0$ axis is at log i_0. If the kinetics are fairly

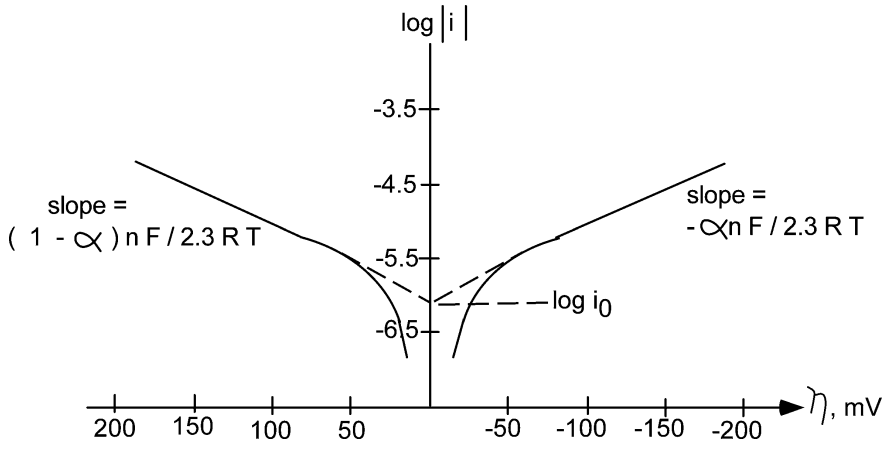

Fig. 7 Tafel plot

fast, no Tafel straight line will be noted, because the mass-transfer-limited current will be reached before the reverse reaction is negligible. Existence of a Tafel region requires that there are no mass-transfer effects. Slow kinetics allow a Tafel region to be observed. Tafel behavior may be used as an indicator of irreversible kinetics, requiring large overpotentials, yielding an essentially unidirectional reaction that is irreversible. The Tafel equation for negative overpotentials is given by:

$$i_{\text{net}} \sim i_0 \exp\left(-\alpha_c \, n f \, \eta\right) \tag{25}$$

As current is passed between a working electrode and reference electrode through an electrolyte, both the working and counter electrodes' potentials move away from their equilibrium values, with one moving positive of its equilibrium value and the other moving negative of its equilibrium value. Total capacitance is proportional to area, with capacitance C_{dl} = (capacitance/area) × area. Capacitance/area is an intrinsic material property. Capacitance is defined as the ability to store charge, and is given by

$$C_{\text{dl}} \equiv \mathrm{d}q/dV \tag{26}$$

where q = charge and V = the electrode potential with respect to some reference electrode

Thus an electrode with a relatively large area and total capacity (as is often the case for a counter electrode) can store a large amount of charge (dq) with a small overpotential (dV). During stimulation, the use of a large counter electrode keeps the potential of the counter electrode fairly constant during charge injection (near its equilibrium value), and there is little Faradaic current (equation 18). Significant overpotentials may be realized at a small working electrode. A typical reason for using a small electrode area is to achieve high spatial resolution during recording or stimulation. It is common to neglect the counter electrode in analysis, and while this is often a fair assumption it is not always the case.

1.6 Ideally Polarizable Electrodes and Ideally Nonpolarizable Electrodes

Two limiting cases for the description of an electrode are the ideally polarizable electrode and the ideally nonpolarizable electrode [8, 9, 14]. The ideally polarizable electrode corresponds to an electrode for which the Z_{faradaic} element has infinite resistance (i.e., this element is absent). Such an electrode is modeled as a pure capacitor, with $C_{\text{dl}} = \mathrm{d}q/\mathrm{d}V$ (equation 26), in series with the solution resistance. In an ideally polarizable electrode, no electron transfer occurs across the electrode/electrolyte interface at any potential when current is passed; rather all current is through capacitive action. No sustained current flow is required to support a large voltage change across the electrode interface. An ideally polarizable electrode is not used as a reference electrode, since the electrode potential is easily perturbed

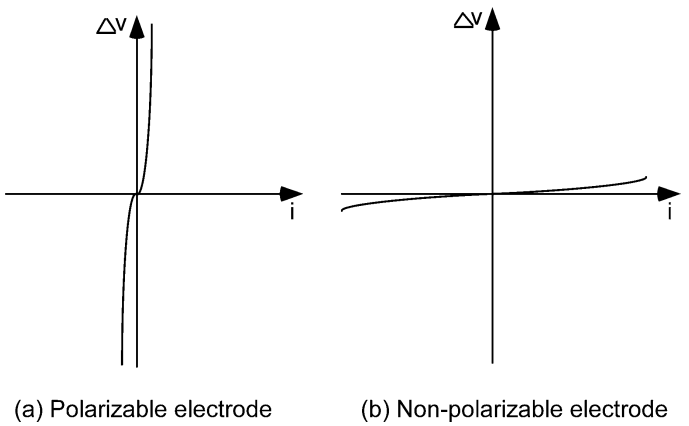

Fig. 8 Current–voltage relationships of highly polarizable and nonpolarizable electrodes

away from the equilibrium potential. A highly polarizable (real) electrode is one that can accommodate a large amount of injected charge on the double layer prior to initiating Faradaic reactions, corresponding to a relatively small exchange current density, e.g., $i_0 = 10^{-9}$ A/cm^2.

The ideally nonpolarizable electrode corresponds to an electrode for which the Z_{faradaic} element has zero resistance; thus only the solution resistance appears in the model. In the ideally nonpolarizable electrode, current flows readily in Faradaic reactions and injected charge is accommodated by these reactions. No change in voltage across the interface occurs upon the passage of current. This is the desired situation for a reference electrode, so that the electrode potential remains near equilibrium even upon current flow. A highly nonpolarizable (real) electrode, for which the Z_{faradaic} element has very small resistance, has a relatively large exchange current density, e.g., $i_0 = 10^{-3}$ A/cm^2. Most real electrode interfaces are modeled by a C_{dl} in parallel with a finite Z_{faradaic}, together in series with the solution resistance (Fig. 3a). Figure 8(a) illustrates a highly polarizable electrode, which rapidly develops a potential upon the passage of current, and Fig. 8(b) illustrates a highly nonpolarizable electrode, which does not readily support a change in potential upon current flow.

Consider a metal electrode consisting of a silver wire placed inside the body, with a solution of silver ions between the wire and ECF, supporting the reaction $Ag^+ + e^- \longleftrightarrow Ag$. This is an example of an electrode of the first kind, which is defined as a metal electrode directly immersed into an electrolyte of ions of the metal's salt. As the concentration of silver ions [Ag^+] decreases, the resistance of the interface increases. At very low silver ion concentrations, the Faradaic impedance Z_{faradaic} becomes very large, and the interface model shown in Fig. 3(a) reduces to a solution resistance R_{S} in series with the capacitance C_{dl}. Such an electrode is an ideally polarizable electrode. At very high silver concentrations, the Faradaic impedance approaches zero and the interface model of Fig. 3(a) reduces to a solution resistance in series with the Faradaic impedance Z_{faradaic}, which is approximated by the solution resistance only. Such an electrode is an ideally nonpolarizable electrode.

The example of a silver electrode placed in direct contact with the ECF, acting as an electrode of the first kind, is impractical. Silver is toxic, silver ions are not innate in the body, and any added silver ions may diffuse away. The silver wire electrode is a highly polarizable electrode since the innate silver concentration is very low and the Faradaic reaction consumes little charge; thus this configuration is not usable as a reference electrode. The equilibrium potential, given by a derivation of the Nernst equation $E_{\text{eq}} = E^{\Theta} + (RT/nF)\ \ln\,[\text{Ag}^+] = (59\ \text{mV/decade})\ \log\,[\text{Ag}^+]$ at 25°C, is poorly defined due to the low silver ion concentration. A solution to these problems is to use an electrode of the second kind, which is defined as a metal coated with a sparingly soluble metal salt. The common silver/silver chloride (Ag/AgCl) electrode, described by reactions 8a and 8b, is such an electrode. This consists of a silver electrode covered with silver chloride, which is then put in contact with the body. The Ag/AgCl electrode acts as a highly nonpolarizable electrode. The equilibrium potential $E_{\text{eq}} = E^{\Theta} + 59\ \log\,[\text{Ag}^+]$ can be combined with the definition of the silver chloride solubility constant:

$K_s \equiv \left[\text{Ag}^+\right]\left[\text{Cl}^-\right] \sim 10^{-10}\text{M}^2$, to yield $E_{\text{eq}} = E^{\Theta} + 59\log\left[K_s/\text{Cl}^-\right] = E^{\Theta} + 59\log K_s - 59\log\left[\text{Cl}^-\right] = E^{\Theta\prime} - 59\log\left[\text{Cl}^-\right]$. The equilibrium potential of this electrode of the second kind is seen to be dependent on the finite chloride concentration rather than any minimal silver concentration, and is well defined for use as a reference electrode.

2 Charge Injection Across the Electrode/Electrolyte Interface During Electrical Stimulation

2.1 Charge Injection During Pulsing: Interaction of Capacitive and Faradaic Mechanisms

As illustrated in Fig. 1, there are two primary mechanisms of charge injection from a metal electrode into an electrolyte. The first consists of charging and discharging the double-layer capacitance causing a redistribution of charge in the electrolyte, but no electron transfer from the electrode to the electrolyte. C_{dl} for a metal in aqueous solution has values on the order of 10–20 $\mu\text{F/cm}^2$ of real area (geometric area multiplied by the roughness factor). For a small enough total injected charge, all charge injection is by charging and discharging of the double layer. Above some injected charge density, a second mechanism occurs consisting of Faradaic reactions where electrons are transferred between the electrode and electrolyte, thus changing the chemical composition in the electrolyte by reduction or oxidation reactions. Figure 1 illustrates a single Faradaic impedance representing the electron transfer reaction $\text{O} + n\,e^- \longleftrightarrow \text{R}$. Generally there may be more than one Faradaic reaction possible, which is modeled by several branches of Z_{faradaic} (one for each reaction), all in parallel with the double-layer capacitance. The current–overpotential equation 18 and Fick's first and second laws for diffusion give the complete description of processes occurring for any Faradaic reaction.

In addition to the double-layer capacitance, some metals have the property of pseudocapacity [8], where a Faradaic electron transfer occurs, but because the product remains bound to the electrode surface, the reactant may be recovered (the reaction may be reversed) if the direction of current is reversed. Although electron transfer occurs, in terms of the electrical model of Fig. 1, the pseudocapacitance is better modeled as a capacitor, since it is a charge-storage (not dissipative) process. Platinum is commonly used for stimulating electrodes, as it has a pseudocapacity (by reaction 6) of 210 $\mu C/cm^2$ real area [18], or equivalently 294 $\mu C/cm^2$ geometric area using a roughness factor of 4.[1]

It is a general principle when designing electrical stimulation systems that one should avoid onset of irreversible Faradaic processes, which may potentially create damaging chemical species, and keep the injected charge at a low enough level where it may be accommodated strictly by reversible charge injection processes. Unfortunately this is not always possible, because a larger injected charge may be required to cause the desired effect (e.g., initiating action potentials). Reversible processes include charging and discharging of the double-layer capacitance, reversible Faradaic processes involving products that remain bound to the surface such as plating of hydrogen atoms on platinum (reaction 6) or the reversible formation and reduction of a surface oxide (reactions 4, 5), and reversible Faradaic processes where the solution phase product remains near the electrode due to mass diffusion limitations.

When the exchange current density is very low and significant overpotentials are required for measurable Faradaic current, a relatively large total charge can be injected (and thus a relatively large overpotential achieved) through the capacitive mechanism before Faradaic reactions commence. When the exchange current density is high, little injected charge is accepted into capacitive charge, and small overpotentials are achieved, before onset of significant Faradaic reactions. The desirable paradigm for a stimulating electrode is to use either capacitive charge injection or charge injection through reversible Faradaic processes (such as reversible oxide formation), thus minimizing irreversible Faradaic reactions that lead to either electrode or tissue damage.

The net current passed by an electrode, modeled as shown in Fig. 1, is the sum of currents through the two parallel branches. The total current through the electrode is given by

$$i_{\text{total}} = i_C + i_{\text{f}} \tag{27}$$

where i_C is the current through the capacitance and i_f is the current through Faradaic processes

[1]The relationship between capacitance and stored charge is given by equation 29. A one volt potential excursion applied to a double layer capacitance of 20 $\mu F/cm^2$ yields 20 $\mu C/cm^2$ stored charge, which is an order of magnitude lower than the total charge storage available from platinum pseudocapacitance.

The current through Faradaic processes is given by the current–overpotential equation 18. The current through the capacitance is given by equation (28) below.

$$i_C = C_{dl}\, dv/dt = C_{dl}\, d\eta/dt \tag{28}$$

The capacitive current depends upon the rate of potential change, but not the absolute value of the potential. The Faradaic current, however, is exponentially dependent upon the overpotential, or departure from the equilibrium potential. Thus, as an electrode is driven away from its equilibrium potential, essentially all charge initially flows through the capacitive branch since the overpotential is small near equilibrium. As the overpotential increases, the Faradaic branch begins to conduct a relatively larger fraction of the injected current. When the overpotential becomes great enough, the Faradaic impedance becomes sufficiently small that the Faradaic current equals the injected current. At this point the Faradaic process of reduction or oxidation conducts all injected charge, and the potential of the electrode does not change, corresponding to the capacitor not charging any further.

In terms of charge going into the different processes, the charge on the double-layer capacitance is proportional to the voltage across the capacitance:

$$q_C = C_{dl} \Delta V \tag{29}$$

thus if the electrode potential does not change in time, neither does the stored charge. The charge into Faradaic processes however does continue to flow for any nonzero overpotential. The Faradaic charge is the integration of Faradaic current over time, which by equation (18) is proportional to an exponential of the overpotential integrated over time:

$$q_f = \int i_f\, dt \;\propto\; \int \exp(\eta)\; dt \tag{30}$$

The charge delivered into Faradaic reactions is directly proportional to the mass of Faradaic reaction product formed, which may be potentially damaging to the tissue being stimulated or the electrode.

2.2 Methods of Controlling Charge Delivery During Pulsing

Charge injection from an electrode into an electrolyte (e.g., extracellular fluid) is commonly controlled by one of three methods. In the current-controlled (also called galvanostatic) method, a current source is attached between the working and counter electrodes and a user-defined current is passed. In the voltage-controlled (also called potentiostatic) method, current is driven between the working electrode and counter electrode as required to control the working electrode potential with respect to a third (reference) electrode. This may be used for electrochemical measurements of certain neurotransmitters [19]. This method is most often not used for stimulation

and is not discussed further in this review. In the third method, $V_{WE\text{-}CE}$ control, a voltage source is applied between the working and counter electrodes. While this is the simplest method to implement, neither the potential of the working electrode nor the potential of the counter electrode (with respect to a third reference electrode) are controlled; only the net potential between the working and counter electrodes is controlled.

2.3 Charge Delivery by Current Control

The current-controlled method is commonly used for electrical stimulation of excitable tissue. This typically takes the form of pulsing. In monophasic pulsing, a constant current is passed for a period of time (generally on the order of tens to hundreds of microseconds), and then the external stimulator circuit is open-circuited (it is effectively electrically removed from the electrodes) until the next pulse. Among the different pulsing schemes, monophasic pulsing results in the greatest amount of irreversible Faradaic reaction product (detailed in the next section), which may result in tissue or electrode damage; thus it is not used in chronic stimulation. In biphasic pulsing, a constant current is passed in one direction, then the direction of current is reversed, and then the circuit is open-circuited until the next pulse. In biphasic pulsing the first phase, or stimulating phase, is used to elicit the desired physiological effect such as initiation of an action potential, and the second phase, or reversal phase, is used to reverse electrochemical processes occurring during the stimulating phase. It is common to use a cathodic pulse as the stimulating phase (the working electrode is driven negative with respect to its prepulse potential), followed by an anodic-reversal phase (the working electrode is driven positive), although anodic pulsing may also be used for stimulation (discussed in Section 4). Figure 9 illustrates definitions of the key parameters in pulsing. The frequency of stimulation is the inverse of the period or time between pulses. The interpulse interval is the period of time between pulses. Figure 9(b) illustrates charge-balanced biphasic pulsing, where the charge in the stimulation phase equals the charge in the reversal phase. Figure 9(c) illustrates charge-imbalanced biphasic pulsing (detailed in Section 4) where there are two phases, but the reversal phase has less charge than the stimulating phase. Figure 9(d) illustrates the use of an interphase delay, where an open-circuit is introduced between the stimulating and reversal phases.

Upon application of a cathodic current pulse to an electrode that starts at a potential close to the equilibrium potential, the term exp (η) is small and initially little charge goes into any Faradaic reactions, thus the initial charge delivery goes into charging the double-layer capacitance. As charge goes onto the double layer, the electrode potential moves away from equilibrium (an overpotential η develops), and the Faradaic reaction $O + ne^- \rightarrow R$ starts to consume charge, with net current density proportional to exp (η). The total injected current then goes into both capacitive current i_c, causing the electrode capacitance to continue to charge to more negative potentials, and Faradaic current i_f. At sufficiently negative potentials, another

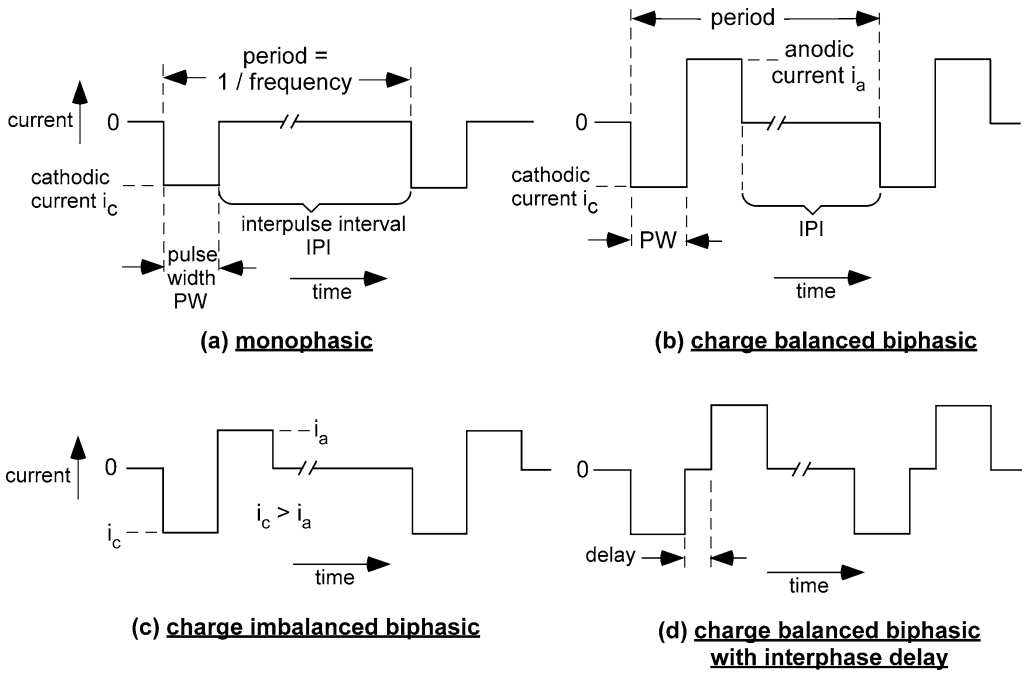

Fig. 9 Common pulse types and parameters

Faradaic reaction with a lower exchange current density (thus more irreversible) than the first may start. In the case where this second reaction is the reduction of water, the reaction will not become mass transport limited (water at 55.5 M will support substantial current), and an electrode potential will be reached where the non-mass transport limited reduction of water accepts all further injected charge. The water window is a potential range that is defined by the reduction of water in the negative direction, forming hydrogen gas, and the oxidation of water in the positive direction, forming oxygen. Because water does not become mass transport limited in an aqueous solution, the potentials where water is reduced and oxidized form lower and upper limits respectively for electrode potentials that may be attained, and any electrode driven to large enough potentials in water will evolve either hydrogen gas or oxygen gas. Upon reaching either of these limits, all further charge injection is accommodated by the reduction or oxidation of water.

2.4 Pulse train response during current control

Based on the simple electrical model of Fig. 1, one may predict different characteristics in the potential waveforms resulting from monophasic pulsing, charge-balanced biphasic pulsing, and charge-imbalanced biphasic pulsing. Consider what occurs when an electrode, starting from the open-circuit potential, is pulsed with a single cathodic pulse and then left open-circuit (illustrated in Fig. 10(a), pulse 1). Upon pulsing the electrode initially charges with injected charge being stored reversibly

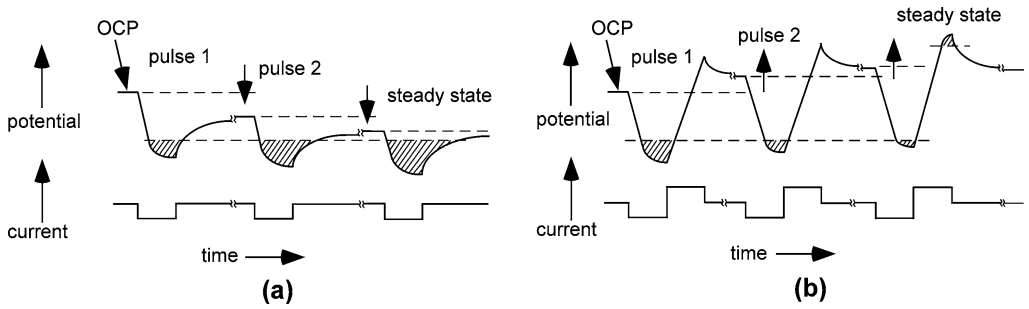

Fig. 10 Electrode Potentials in Response to Monophasic and Charge-Balanced Biphasic Pulse Trains (**a**) Ratcheting of potential during monophasic cathodic pulsing. The prepulse potential of successive pulses moves negative until all injected charge goes into irreversible processes. (**b**) Ratcheting during charge-balanced cathodic first biphasic pulsing. The prepulse potential of successive pulses moves positive until the same amount of charge is lost irreversibly during the cathodic and anodic phases. Shaded areas represent periods of irreversible reactions

on the double-layer capacitance, causing the electrode potential to move negative. As the potential continues to move negative, charge begins to be delivered into Faradaic currents (whose magnitude is an exponential function of the overpotential). At the end of the pulse when the external circuit is opened, charge on the double-layer capacitance continues to discharge through Faradaic reactions. This causes the electrode potential to move positive, and as the electrode discharges (i.e., the overpotential decreases) the Faradaic current decreases, resulting in an exponential discharge of the electrode. Given a long enough time, the electrode potential will approach the open-circuit potential. However, if the electrode is pulsed with a train whose period is short with respect to the time constant for discharge (as may occur with neural stimulation, with a period of perhaps 20 ms), i.e., if a second cathodic pulse arrives before the electrode has completely discharged, then the potential at the start of the second pulse (the prepulse potential) is more negative than the prepulse potential of the first pulse (which is the open circuit potential). Because the potential during the second pulse begins at a more negative potential than the first, a smaller fraction of the injected charge goes into reversible charging of the double-layer capacitance. The Faradaic reactions begin accepting significant charge at an earlier time than in the first pulse, and there is more charge delivered to irreversible reactions during the second pulse than during the first as the overall potential range traversed is more negative during the second pulse (Fig. 10(a), pulse 2). Upon going to open-circuit after the second pulse, the electrode discharges through Faradaic reactions. Because the potential at the end of the second current pulse is more negative than the potential at the end of the first current pulse, the potential range during discharge between pulses 2 and 3 is also more negative than between pulses 1 and 2, and likewise the prepulse potential of pulse 3 is more negative than the prepulse potential of pulse 2. This "ratcheting" of the electrode potential continues until the following condition is met:

$$\text{Unrecoverable Charge } (Q_{\text{ur}}) \text{ per pulse} = \text{Injected Charge } \left(Q_{\text{inj}}\right) \text{ per pulse} \quad (31)$$

i.e., all injected charge goes into irreversible Faradaic reactions that occur either during the pulse or during the open-circuit interpulse interval period. Charge delivered into irreversible processes is defined as unrecoverable charge Q_{ur}. Once condition (31) is met, the pulsing is in the steady state, and the potential excursions repeat themselves with each pulse cycle.

Next consider the electrode response when a charge-balanced stimulation protocol is used; cathodic then anodic, followed by open-circuit. The electrode begins from open-circuit potential. Upon applying the first cathodic pulse, the double-layer reversibly charges, and then the electrode may begin to transfer charge into Faradaic reactions as the potential moves negative. The anodic pulse then causes the electrode potential to move back positive (illustrated in Fig. 10(b), pulse 1). Unlike the exponential decay during the monophasic pulsing, the electrode potential now changes according to the anodic current and the double-layer capacitance, and there is reversal of charge from the double layer. Because not all of the injected charge during the cathodic pulse went into charging of the double layer, only some fraction of the injected cathodic charge is required in the anodic phase to bring the electrode potential back to the prepulse value. Since the anodic pulse is balanced with the cathodic pulse, the electrode potential at the end of the anodic phase of pulse 1 is positive of the prepulse potential of pulse 1 (the open circuit potential). During the anodic phase and during the open-circuit following the anodic phase, if the potential becomes sufficiently positive, anodic Faradaic reactions such as electrode corrosion may occur. During the open-circuit period, the electrode discharges exponentially through anodic Faradaic reactions back toward the open-circuit potential, moving negative with time. By the beginning of pulse 2, the potential is still positive of the prepulse potential for pulse 1 (the open-circuit potential). Thus, as long as any charge is lost irreversibly during the cathodic phase, the potential at the end of the charge-balanced anodic phase will be positive of the prepulse potential, and a ratcheting effect is seen. Unlike the monophasic case, the ratcheting of the electrode prepulse potential is now in a positive direction. Steady state occurs when one of the two following conditions is met:

(1) *There are no irreversible Faradaic reactions during either the cathodic or anodic phases, and the electrode simply charges and then discharges the double layer (the potential waveform appears as a sawtooth):*

$$Q_{\text{ur cathodic}} = Q_{\text{ur anodic}} = 0 \tag{32}$$

or

(2) *The same amount of charge is lost irreversibly during the cathodic phase and during the combined anodic phase and interpulse interval:*

$$Q_{\text{ur cathodic}} = Q_{\text{ur anodic+IPI}} \neq 0 \tag{33}$$

If irreversible processes do occur, for cathodic first charge-balanced biphasic pulsing, the electrode potential will move positive of the open-circuit potential, and during steady-state continuous pulsing there is an equal amount of unrecoverable charge delivered into cathodic- and anodic-irreversible processes.

Finally consider the electrode response when a charge-imbalanced stimulation protocol is used (not illustrated). The electrode begins from open-circuit potential. The response to the first cathodic pulse is the same as with the monophasic or charge-balanced biphasic waveforms. The anodic phase then causes the electrode potential to move back positive, but since there is less charge in the anodic phase than cathodic, the electrode potential does not move as far positive as it did with the charge-balanced biphasic waveform. The potential at the end of the anodic phase will be closer to the open-circuit potential than during charge-balanced pulsing. The maximum positive potential will be less when using the charge-imbalanced waveform than when using the charge-balanced waveform. This has the advantage that charge delivered into anodic Faradaic processes such as metal corrosion is reduced with respect to charge-balanced stimulation. The prepulse potential will move under factors as explained for the monophasic and charge-balanced biphasic waveforms until the following condition is met:

The net imbalance in injected charge is equal to the net difference in unrecoverable charge between the cathodic phase and the combined anodic phase and interpulse interval:

$$(Q_{\text{inj cathodic}} - Q_{\text{inj anodic}}) \equiv Q_{\text{imbal}} = (Q_{\text{ur cathodic}} - Q_{\text{ur anodic}+IPI}) \quad (34)$$

During charge-imbalanced stimulation, the shift in prepulse potential may be either positive or negative of the open-circuit potential depending on the amount of imbalance.

Based on these considerations, monophasic pulsing causes the greatest shift of the electrode potential during pulsing away from the equilibrium potential, thus causes the most accumulation of unrecoverable charge (corresponding to products of irreversible Faradaic reactions) of the three protocol types (monophasic, charge-balanced biphasic, charge-imbalanced biphasic). Furthermore, since during monophasic pulsing the electrode potential is not brought back toward the equilibrium potential by an anodic phase, there is accumulation of unrecoverable charge during the open-circuit interpulse interval.

2.5 Electrochemical reversal

The purpose of the reversal phase during biphasic stimulation is to reverse the direction of electrochemical processes that occurred during the stimulating phase, minimizing unrecoverable charge. A reversible process is one where the reactants are reformed from the products upon reversing the direction of current. Upon delivering current in the stimulation phase and then reversing the direction of current,

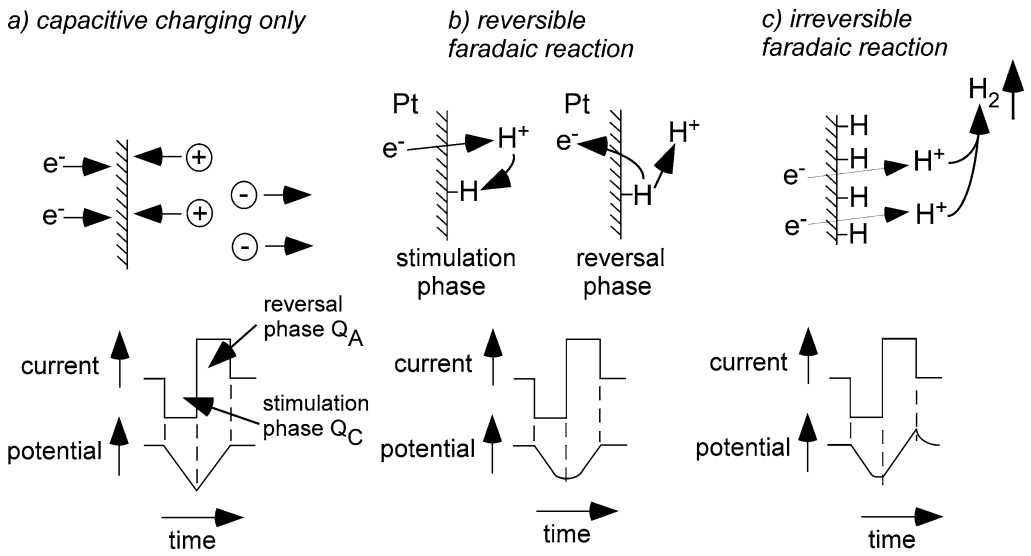

Fig. 11 Electrochemical Processes and Potential Waveforms During Charge-Balanced Stimulation (**a**) capacitive charging only (**b**) reversible hydrogen plating (**c**) irreversible hydrogen evolution

charge on the electrode capacitance will discharge, returning the electrode potential toward its prepulse value. If only double-layer charging occurred, then upon passing an amount of charge in the reversal phase equal to the charge delivered in the stimulation phase (a charge-balanced protocol), the electrode potential will return precisely to its prepulse potential by the end of the reversal phase and the potential curve will be a simple sawtooth as shown in Fig. 11(a) (corrected for solution resistance). If reversible Faradaic reactions occur during the stimulation phase, then charge in the reversal or secondary phase may go into reversing these reactions. Figure 11(b) illustrates an example reversible Faradaic process; in this case, charging of the pseudocapacitance (reduction of protons and plating of monatomic hydrogen onto the metal electrode surface) as may occur on platinum. During reversal, the plated hydrogen is oxidized back to protons. Because the electrochemical process occurring during the reversal phase is the exact opposite of that occurring during the stimulation phase, there is zero net accumulation of electrochemical species. Reversible Faradaic reactions include adsorption processes as in Fig. 11(b), as well as processes where the solution-phase product remains near the electrode due to mass-diffusion limitations. If irreversible Faradaic reactions occur, upon passing current in the reverse direction, reversal of electrochemical product does not occur as the product is no longer available for reversal (it has diffused away). An example shown in Fig. 11(c) is the formation of hydrogen gas after a monolayer of hydrogen atoms has been adsorbed onto the platinum surface. In the case where a Faradaic reaction has occurred during the stimulation phase, the potential waveform during the stimulation phase is not linear, but displays a slope inflection as Faradaic processes consume charge (this is charge that does *not* charge the capacitance, thus does not change the electrode potential). If irreversible Faradaic reactions occur,

then when an equal amount of charge is passed in the reversal phase, the electrode potential goes positive of the prepulse potential. To return the electrode potential exactly to its prepulse value would require that the charge in the reversal phase be equal to only the amount of charge that went onto the capacitance during the stimulation phase (a charge-imbalanced waveform).

The use of biphasic stimulation (either charge balanced or charge imbalanced) moves the electrode potential out of the most negative ranges immediately after stimulation. In comparison (as shown in Fig. 10), the monophasic-stimulation protocol allows the electrode potential to remain relatively negative during the interpulse interval, and during this time Faradaic reduction reactions may continue. In the presence of oxygen, these reactions may include reduction of oxygen and formation of reactive oxygen species, which have been implicated in tissue damage [20, 21, 22, 23, 24]. The charge-imbalanced waveform has the added advantage that the electrode potential at the end of the anodic pulse is less positive than with charge-balanced biphasic pulsing, thus less charge goes into irreversible oxidation reactions such as corrosion when using the charge-imbalanced protocol. Charge-imbalanced biphasic waveforms provide a method to reduce unrecoverable charge in the cathodic direction (with respect to monophasic stimulation) and in the anodic direction (with respect to charge-balanced biphasic stimulation), thus are an attractive solution to minimizing damage to either the stimulated tissue or the metal electrode.

2.6 Charge delivery by a voltage source between the working electrode and counter electrode

An alternative form of charge injection involves the direct connection of a voltage source between the working and counter electrodes. Figure 12 compares the current, working electrode to reference electrode voltage ($V_{\text{WE-RE}}$), and working electrode to counter electrode voltage ($V_{\text{WE-CE}}$) waveforms during monophasic pulsing under current control versus $V_{\text{WE-CE}}$ control. The $V_{\text{WE-RE}}$ waveforms represent the working electrode interfacial potentials and do not imply that a reference electrode is required for either control scheme. Upon applying a voltage pulse with amplitude V_{app} between the working electrode and counter electrode in $V_{\text{WE-CE}}$ control, the current is at its maximum value at the beginning of the pulse as the double-layer capacitances of the two electrodes charge and the current is predominantly capacitive. Given a long duration pulse, the current will asymptotically approach a value where V_{app} maintains a steady-state Faradaic current, with current density given by equation (18). Figure 12 illustrates the steady-state waveforms when using an exhausting circuit [25, 26], where at the end of the monophasic voltage pulse the working and counter electrodes are shorted together, causing the charge on the working electrode capacitance to rapidly discharge, and the working electrode potential to attain the counter electrode potential. If the counter electrode is sufficiently large, its potential will not be notably perturbed away from its equilibrium potential during pulsing, and upon shorting the working electrode to the counter electrode, the

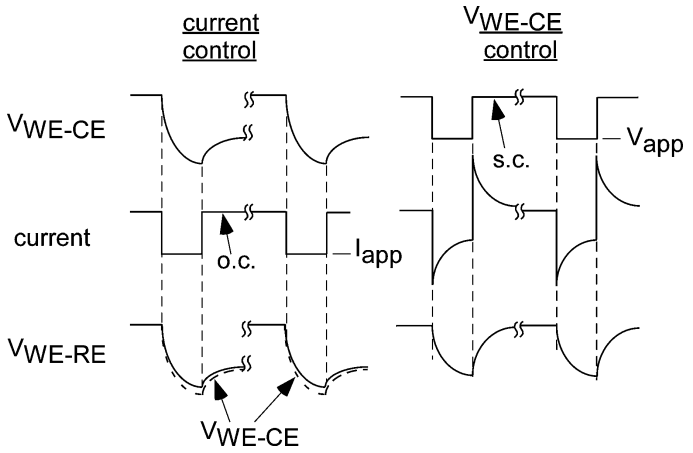

Fig. 12 Steady-State Voltage and Current Waveforms Using Current Control and $V_{\text{WE-CE}}$ Control Note the rapid discharge of the working electrode during the short-circuit interpulse interval of $V_{\text{WE-CE}}$ control relative to the open-circuit interpulse interval of current control. s.c.=short circuit, o.c.=open circuit, I_{app}=applied current, V_{app}=applied voltage

working electrode potential will be brought back to the counter electrode equilibrium potential. Donaldson [26] showed that during cathodic-monophasic pulsing of real electrodes with an exhausting scheme, the potentials of both the working electrode and counter electrode moved positive in response to a continuous train, increasing the risk of oxidizing reactions such as corrosion. The discharge of the working electrode is relatively rapid during $V_{\text{WE-CE}}$ control with an exhausting circuit, as the working electrode is directly shorted to the counter electrode. This is contrasted by the relatively slow discharge using monophasic current control, as shown in Fig. 12, with an open circuit during the interpulse interval. During the open-circuit period, the working-electrode capacitance discharges through Faradaic reactions at the working-electrode interface. This leads to a greater accumulation of unrecoverable charge during the open-circuit interpulse interval (current control) than with the short-circuit interpulse interval ($V_{\text{WE-CE}}$ control). However, in current control, appropriate biphasic pulsing waveforms (Fig. 9) can promote rapid electrode discharge.

Advantages of the $V_{\text{WE-CE}}$ control scheme over the current control scheme include (1) the circuitry is simpler (it may be a battery and an electronic switch); and (2) unrecoverable charge accumulation is lower during the interpulse interval than it would be with monophasic current control. Disadvantages of the $V_{\text{WE-CE}}$ control scheme include (1) maximum stimulation of excitable tissue occurs only at the beginning of the pulse when current is maximum, and stimulation efficiency decreases throughout the pulse as current decreases, whereas with current control the current is constant throughout the pulse; (2) an increase in resistance anywhere in the electrical conduction path will cause an additional voltage drop, decreasing the current and potentially causing it to be insufficient for stimulation, whereas with current control the current is constant (assuming the required voltage is within the range of the stimulator); and (3) neither the current driven nor the charge injected

are under direct control using voltage control [27]. Because the level of neuronal membrane depolarization is related to the applied current, these factors result in a reduction in reproducibility between experiments, as well as between clinical implants, during $V_{\text{WE-CE}}$ control. Moreover, because tissue properties can change over time, stimulation efficacy may change when using $V_{\text{WE-CE}}$ control.

3 Materials Used as Electrodes for Charge Injection and Reversible Charge Storage Capacity

The ideal material for use as a stimulating electrode satisfies the following six requirements. (1) The passive (unstimulated) material must be biocompatible, so it should not induce a toxic or necrotic response in the adjacent tissue, nor an excessive foreign body or immune response. (2) The material must be mechanically acceptable for the application. It must maintain mechanical integrity given the intended tissue, surgical procedure, and duration of use. The material must not buckle if it is to pass through the meninges. If a device is to be used chronically, it must be flexible enough to withstand any small movement between the device and tissue following implantation. (3) The complete device must be efficacious. This requires that sufficient charge can be injected with the chosen material and electrode area to elicit action potentials. The required charge is quantified by the charge-duration curve, discussed in Section 4. (4) During electrical stimulation, Faradaic reactions should not occur at levels that are toxic to the surrounding tissue. The level of reaction product that is tolerated may be significantly higher for acute stimulation than chronic stimulation. (5) During electrical stimulation, Faradaic corrosion reactions should not occur at levels that will cause premature failure of the electrode. This again depends greatly on the intended duration of use. During acute stimulation, corrosion is rarely a concern, whereas a device that is intended for a 30-year implant must have a very low corrosion rate. (6) The material characteristics must be acceptably stable for the duration of the implant. For a chronic electrode, the device electrical impedance must be stable. The conducting and insulating properties of all materials must remain intact.

Dymond et al. [28] tested the toxicity of several metals implanted into the cat cerebral cortex for 2 months. Materials were deemed toxic if the reaction to the implanted metal was significantly greater than the reaction to a puncture made from the same metal that was immediately withdrawn (Table 1). Stensaas and Stensaas [29] reported on the biocompatibility of several materials implanted passively into the rabbit cerebral cortex (Table 1). Materials were classified into one of three categories depending upon changes occurring at the implant/cortex interface: (1) Nonreactive. For these materials, little or no gliosis occurred, and normal CNS tissue with synapses was observed within 5 μm of the interface. (2) Reactive. Multinucleate giant cells and a thin layer (10 μm) of connective tissue surrounded the implant. Outside of this was a zone of astrocytosis. Normal CNS tissue was observed within 50 μm of the implant. (3) Toxic. These materials are separated from the cortical tissue by a capsule of cellular connective tissue and a surrounding zone

Table 1 Classification of material biocompatibility

	Classification by Dymond	Classification by Stensaas and Stensaas	Other references
Conductors:			
Aluminum		Non-reactive	
Cobalt		Toxic	
Copper		Toxic	Toxic [34, 35, 36]
Gold	Nontoxic	Non-reactive	
Gold-nickel-chromium	Nontoxic		
Gold-palladium-rhodium	Nontoxic		
Iron		Toxic	
Molybdenum		Reactive	
Nickel-chromium (Nichrome)		Reactive	Nontoxic [34]
Nickel-chromium-molybdenum	Nontoxic		
Nickel-titanium (Nitinol)			Biocompatible [37, 38]
Platinum	Nontoxic	Non-reactive	Biocompatible [31, 32]
Platinum-iridium	Nontoxic		Biocompatible [33]
Platinum-nickel	Nontoxic		
Platinum-rhodium	Nontoxic		
Platinum-tungsten	Nontoxic		
Platinized platinum (Pt black)	Nontoxic		
Rhenium	Nontoxic		
Silver	Toxic	Toxic	Toxic [34, 35, 36]
Stainless steel	Nontoxic		Nontoxic [34]
Tantalum		Reactive	
Titanium			Biocompatible [32]
Tungsten		Non-reactove	
Insulators:			
Alumina ceramic		Non-reactive	Biocompatible [32]
Araldite (epoxy plastic resin)		Reactive	
Polyethylene		Non-reactive	
Polyimide			Biocompatible [154]
Polypropylene		Non-reactive	
Silastic RTV	Toxic		
Silicon dioxide (Pyrex)		Reactive	
Teflon TFE (high purity)		Non-reactive	
Teflon TFE (shrinkable)		Reactive	
Titanium dioxide		Reactive	
Semiconductors:			
Germanium		Toxic	
Silicon		Non-reactive	Biocompatible [40, 155, 156]
Assemblies			
Gold-silicon dioxide passivated microcircuit		Reactive	

of astrocytosis. Loeb [30] studied the histological response to materials used by the microelectronics industry implanted chronically in the subdural space of cats, and found reactions to be quite dependent on specific material formulations and surface preparations.

Platinum has been demonstrated as biocompatible for use in an epiretinal array [31] and in cochlear implants [32]. Both titanium and ceramic [32] and platinum-iridium wire [33] have been shown as biocompatible in cochlear implants. Babb and Kupfer [34] have shown stainless steel and nickel-chromium (Nichrome) to be nontoxic. Copper and silver are unacceptable as stimulating electrodes, as these metals cause tissue necrosis even in the absence of current [28, 29, 34, 35, 36]. Nickel-titanium shape memory alloys have good biocompatibility response [37], up to a nickel content of 50% [38].

The first intracortical electrodes consisted of single-site conductive microelectrodes made of material stiff enough to penetrate the meninges, as either an insulated metallic wire or a glass pipette filled with conductive electrolyte. Advances in materials science and microelectronics technology have allowed the development of multiple-site electrodes built onto a single substrate using planar photolithographic and silicon micromachining technologies. Such devices have been made from silicon [39, 40] and polyimide [41]. In further advancements, bioactive components have been added to the electrode to direct neurite growth toward the electrode, minimizing the distance between the electrode and stimulated tissue [42, 43, 44].

Chronic implantation of any device into the central nervous system, even those materials considered biocompatible, elicits a common response consisting of encapsulation by macrophages, microglia, astrocytes, fibroblasts, endothelia, and meningeal cells [45]. The early response to material implantation is inflammation [29, 45, 46]. The chronic response is characterized by a hypertrophy of the surrounding astrocytes [29], which display elevated expression of intermediate filament proteins such as GFAP and vimentin [47], an infiltration of microglia and foreign body giant cells [29], and a thickening of the surrounding tissue that forms a capsule around the device [40, 46].

The reversible charge-storage capacity (CSC) of an electrode, also known as the reversible charge injection limit [48], is the total amount of charge that may be stored reversibly, including storage in the double-layer capacitance, pseudocapacitance, or any reversible Faradaic reaction. In electrical stimulation of excitable tissue, it is desirable to have a large reversible charge-storage capacity so that a relatively large amount of charge may be injected (thus being efficacious for stimulation) prior to the onset of irreversible Faradaic reactions (which may be deleterious to the tissue being stimulated or to the electrode itself). The reversible charge-storage capacity depends upon the material used for the electrode, the size and shape of the electrode, the electrolyte composition, and parameters of the electrical stimulation waveform.

The slow cyclic voltammogram for a material is a graphic display of the current density into various electrochemical processes as a function of the electrode potential as the potential is slowly cycled. At any point in time, the amount of current going into a particular process is determined by the potential as well as by the

reactant concentration, as given by equation (18). The water window is defined as the potential region between the oxidation of water to form oxygen and the reduction of water to form hydrogen. Because water does not become mass transport limited in an aqueous solution, once the electrode potential attains either of these two water-window boundaries, all further injected charge goes into the irreversible processes of water oxidation (anodically) or water reduction (cathodically). In many studies, the reversible charge-storage capacity has been defined as the maximum charge density that can be applied without the electrode potential exceeding the water window during pulsing. It should be noted that in fact irreversible processes might occur at potentials within the water window, including such reactions as irreversible oxygen reduction [49, 50] that may become mass transport limited.

The noble metals, including platinum Pt, gold Au, iridium Ir, palladium Pd, and rhodium Rh, have been commonly used for electrical stimulation, largely due to their relative resistance to corrosion [28, 51, 52]. These noble metals do exhibit some corrosion during electrical stimulation, as shown by dissolution [53, 54, 55, 56, 57] and the presence of metal in the neighboring tissue [58, 59]. In addition to corrosion of the electrode, there is evidence of long-term toxic effects on the tissue from dissolution [60, 61, 62].

Platinum and platinum-iridium alloys are common materials used for electrical stimulation of excitable tissue. Brummer and Turner [63, 64, 65, 66] have reported on the electrochemical processes of charge injection using a platinum electrode. They reported that three processes could store charge reversibly, including charging of the double-layer capacitance, hydrogen atom plating and oxidation (pseudocapacity, reaction 6), and reversible oxide formation and reduction on the electrode surface, and that 300–350 $\mu C/cm^2$ (real area) could theoretically be stored reversibly by these processes in artificial cerebrospinal fluid (equivalently 420–490 $\mu C/cm^2$ (geometric area)). This is a maximum reversible charge-storage capacity under optimum conditions, including relatively long pulse widths (>0.6 ms). Rose and Robblee [67] reported on the charge-injection limits for a platinum electrode using 200 μs charge-balanced biphasic pulses. The reversible charge-injection limit was defined as the maximum charge density that could be applied without the electrode potential exceeding the water window during pulsing. The authors determined the charge-injection limit to be 50–100 $\mu C/cm^2$ (geometric) using anodic first pulses, and 100–150 $\mu C/cm^2$ (geometric) using cathodic first pulses. These values are considerably lower than the theoretical values determined by Brummer and Turner [66], since the electrode potential at the beginning of a pulse begins somewhere intermediate to oxygen and hydrogen evolution and not all of the three reversible processes accommodate charge during the stimulating pulse. Dissolution of platinum in saline increases linearly with the injected charge during biphasic stimulation [55]. Anodic first pulses cause more dissolution than cathodic first pulses, as the electrode potential attains more positive values during the stimulating (first) phase. Robblee et al. [56] have shown that in the presence of protein such as serum albumin, the dissolution rate of platinum decreases by an order of magnitude.

The reversible charge-storage capacity is dependent upon the electrode real surface area and geometry. The geometric area of an electrode is usually easily

calculated, but the real area is the value that determines the total charge capacity. Brummer and Turner [65] have reported on a method to experimentally determine the real area of a platinum electrode in vitro, however this may not be applicable to the in vivo situation. It should also be noted that the real area of an electrode may change during the course of stimulation. A nonuniform (nonspherical) electrode geometry will cause a nonuniform current density [68] with maximum current at the electrode edges, which may lead to localized electrode corrosion [69] or tissue burns [70] at the electrode edges.

Platinum is a relatively soft material and may not be mechanically acceptable for all stimulation applications. Platinum is often alloyed with iridium to increase the mechanical strength. Alloys of platinum with 10–30% iridium have similar charge-storage capacity to pure platinum [57]. Iridium is a much harder metal than platinum, with mechanical properties that make it suitable as an intracortical electrode. The reversible charge-storage capacities of bare iridium or rhodium are similar to that of platinum. However, when a surface oxide is present on either of these materials, they have greatly increased charge-storage capacity over platinum. These electrodes inject charge using valency changes between two oxide states, without a complete reduction of the oxide layer.

Iridium oxide is a popular material for stimulation and recording, using reversible conversion between Ir^{3+} and Ir^{4+} states within an oxide to achieve high reversible charge-storage capacity. Iridium oxide is commonly formed from iridium metal in aqueous electrolyte by electrochemical activation (known as anodic iridium oxide films on bulk iridium metal, or AIROF), which consists of repetitive potential cycling of iridium to produce a multilayered oxide [10, 48, 57, 71, 72]. Such activated iridium oxide films have been used for intracortical stimulation and recording using iridium wire [73, 74, 75, 76, 77] or with micromachined silicon electrodes using sputtered iridium on the electrode sites [78, 79]. The maximum charge density that can be applied without the electrode potential exceeding the water window was reported for activated iridium oxide using 200 μs charge-balanced pulses as +/−2 mC/cm^2 (geometric) for anodic first pulsing and −/+1 mC/cm^2 for cathodic first [80, 81]. By using an anodic bias, cathodic charge densities of 3.5 mC/cm^2 (geometric) have been demonstrated both in vitro [80, 81] and in vivo [82]. Iridium oxide films can also be formed by thermal decomposition of an iridium salt onto a metal substrate (known as thermally prepared iridium oxide films, or TIROF) [83], or by reactive sputtering of iridium onto a metal substrate (known as sputtered iridium oxide films, or SIROF) [84]. Meyer and Cogan [77] reported on a method to electrodeposit iridium oxide films onto substrates of gold, platinum, platinum-iridium, and 316LVM stainless steel achieving reversible charge-storage capacities of >25 mC/cm^2.

The stainless steels (types 303, 316, and 316LVM) as well as the cobalt-nickel-chromium-molybdenum alloy MP35N are protected from corrosion by a thin passivation layer that develops when exposed to atmospheric oxygen and which forms a barrier to further reaction. In the case of stainless steel, this layer consists of iron oxides, iron hydroxides, and chromium oxides. These metals inject charge by reversible oxidation and reduction of the passivation layers. A possible problem with these metals is that if the electrode potential becomes too positive

(the transpassive region), breakdown of the passivation layer and irreversible metal dissolution may occur at an unacceptable rate [51, 85, 86], potentially leading to failure of the electrode. A cathodic charge imbalance has been shown to allow significantly increased charge injection without electrode corrosion [87, 88]. Titanium and cobalt-chromium alloys are also protected from corrosion by a surface oxide passivation layer and demonstrate better corrosion resistance than does stainless steel [89]. 316LVM stainless steel has good mechanical properties and has been used for intramuscular electrodes. The charge-storage capacity of 316LVM is only 40–50 $\mu C/cm^2$ (geometric), potentially necessitating large surface area electrodes.

Capacitor electrodes inject charge strictly by capacitive action, as a dielectric material separates the metal electrode from the electrolyte preventing Faradaic reactions at the interface [90, 91, 92]. The tantalum/tantalum pentoxide (Ta/Ta_2O_5) electrode has a high charge-storage capacity achieved by using sintered tantalum or electrolytically etched tantalum wire to increase the surface area [93]. Guyton and Hambrecht [90, 91] have demonstrated a sintered Ta/Ta_2O_5 electrode with a charge-storage capacity of 700 $\mu C/cm^2$ (geometric). The Ta/Ta_2O_5 electrodes have sufficient charge-storage capacity for electrodes in the range of 0.05 cm^2 and charge densities up to 200 $\mu C/cm^2$ (geometric); however, they may not be acceptable for microelectrode applications where the required charge densities may exceed 1 mC/cm^2 [92]. Tantalum capacitor electrodes must operate at a relatively positive potential to prevent electron transfer across the oxide. If pulsed cathodically, a positive bias must be used on the electrode.

Stimulation of muscle, peripheral nerve, or cortical surface requires relatively high charge per pulse (on the order of 0.2–5 μC), thus platinum or stainless steel electrodes must be of fairly large surface area to stay within the reversible charge-storage capacity. Intracortical stimulation requires much less total charge per pulse; however, in order to achieve selective stimulation, the electrode size must be very small, resulting in high charge-density requirements. With a geometric surface area of $20 \times 10^{-6} cm^2$, the charge per pulse may be on the order of 0.008–0.064 μC yielding a charge density of 400–3200 $\mu C/cm^2$ [82, 94]. Such high charge densities may be achieved using iridium oxide electrodes with anodic pulses, or cathodic pulses with an anodic bias.

Table 2 lists several parameters of interest for materials commonly used for stimulation.

4 Charge Injection for Extracellular Stimulation of Excitable Tissue

The goal of electrical stimulation of excitable tissue is often the triggering of action potentials in axons, which requires the artificial depolarization of some portion of the axon membrane to threshold. In the process of extracellular stimulation, the extracellular region is driven to relatively more negative potentials, equivalent to driving the intracellular compartment of a cell to relatively more positive potentials. Charge is transferred across the membrane due to both passive (capacitive and resistive) membrane properties as well as through active ion channels [95]. The process

Table 2 Reversible charge-storage capacity and other parameters in electrode material selection

	Reversible charge Storage capacity ($\mu C/cm^2$)	Reversible charge injection processes	Corrosion characteristics	Mechanical characteristics
Platinum				
AF, 200 μs:	300–350 r [66]	double layer charging, hydrogen atom plating, and oxide formation and reduction	relatively resistant; greatly increased resistance with protein	relatively soft
CF, 200 μs:	50–100 g [67]			
	100–150 g [67]			
Platinum/Iridium Alloys	Similar CSC to Pt			stronger than Pt
Iridium	Similar CSC to Pt			stronger than Pt
Iridium Oxide				
	AF: +/− 2200 g [80, 81]	Oxide valency charges	highly resistant [57, 82]	
	CF: −/+ 1200 g [80, 81]			
	AB: −/+ 3500 g [80, 81, 82]			
316LVM Stainless Steel	40−50 g	passive film formation and reduction	resistant in passive region; rapid breakdown in transpassive region	strong and flexible
Tantalum/ Tantalum Pentoxide	700 g [90, 91]	capacitive only	corrosion resistant [93, 157, 158, 159]	
	200 g [92]			

r = real area, g = geometric area, AF = anodic first, charge-balanced CF = cathodic first, charge-balanced AB = cathodic first, charge balanced, with anodic bias.

of physiological action-potential generation is well reviewed in the literature (in particular, see Principles of Neural Science by Kandel, Schwartz, and Jessell, 2000) [96]), and models have been proposed [97, 98] for mammalian myelinated axons in terms of the parameters "m" and "h" as defined by Hodgkin and Huxley [99, 100, 101, 102] in their studies of the squid giant axon.

The mechanisms underlying electrical excitation of nerve have been reviewed elsewhere [1, 103, 104, 105, 106]. In the simplest case of stimulation, a monopolar electrode (a single current carrying conductor) is placed in the vicinity of excitable tissue. Current passes from the electrode, through the extracellular fluid surrounding the tissue of interest, and ultimately to a distant counter electrode. For a current I (in amps) flowing through the monopolar electrode located a distance r away from a segment of excitable tissue, and uniform conductivity in the fluid of σ (S/m), the extracellular potential V_e at the tissue is

$$V_e = \frac{I}{4\pi\sigma r} \tag{35}$$

Bipolar and other electrode configurations have more complex voltage and current patterns and will not be discussed here. Durand [106] has reviewed solutions for electrical-potential profiles of various systems.

During current-controlled stimulation, the current is constant throughout the period of the pulse; thus the V_e at any point in space is constant during the pulse. During $V_{WE\text{-}CE}$ control, current is not constant throughout the period of the pulse (Fig. 12) and the V_e at any point decreases during the pulse.

The electric field generated by a monopolar electrode will interact with an axon membrane (these principles may be generalized to any excitable tissue). During cathodic stimulation, the negative charge of the working electrode causes a redistribution of charge on the axon membrane, with negative charge collecting on the outside of the membrane underneath the cathode (depolarizing the membrane). Associated with the depolarization of the membrane under the cathode is movement of positive charge intracellularly from the distant axon to the region under the electrode, and hyperpolarization of the membrane at a distance away from the electrode. If the electrode is instead driven as an anode (to more positive potentials), hyperpolarization occurs under the anode, and depolarization occurs at a distance away from the anode. During such anodic stimulation, action potentials may be initiated at the regions distant from the electrode where depolarization occurs, known as virtual cathodes. The depolarization that occurs with anodic stimulation is roughly 1/7–1/3 that of the depolarization with cathodic stimulation; thus cathodic stimulation requires less current to bring an axon to threshold. During cathodic stimulation, anodic surround block may occur at sufficiently high current levels where the hyperpolarized regions of the axon distant from the cathode may suppress an action potential that has been initiated near the electrode. This effect is observed at higher current levels than the threshold values required for initiation of action potentials with cathodic stimulation.

In a mammalian axon, hyperpolarizing with a pulse that is long compared with the time constant of the sodium inactivation gate will remove the normal partial inactivation. If the hyperpolarizing current is then abruptly terminated (as with a rectangular pulse), the sodium activation gate conductance increases back to the rest value relatively quickly, but the activity of the slower inactivation gate remains high for a period of milliseconds; thus the net sodium conductance is briefly higher than normal and an action potential may be initiated. This phenomenon, known as anodic break, may be observed with either cathodic or anodic stimulation, since both cause some region of hyperpolarization in the axon. Anodic break may be prevented by using stimulating waveforms with slowly decaying exponential phases instead of abrupt terminations [107, 108, 109, 110].

Prolonged subthreshold stimuli can produce the phenomenon of accommodation. A long-duration cathodic pulse to mammalian axon that produces subthreshold depolarization will increase sodium inactivation, reducing the number of axons that can be recruited and so increasing the threshold. This is not a problem with brief pulses that are shorter than the time constant of sodium channel inactivation, but can be with more prolonged pulses.

It is often desirable to have some degree of selectivity during electrical excitation of tissue. Selectivity is the ability to activate one population of neurons

without activating a neighboring population. Spatial selectivity is the ability to activate a localized group of neurons, such as restricting activation to a certain fascicle or fascicles within a nerve trunk. Changes in the transmembrane potential due to electrical excitation are greatest in fibers closest to the stimulating electrode because the induced extracellular potential decreases in amplitude with distance from the stimulation electrode (equation 35), as does the second spatial derivative of the extracellular potential, which is responsible for excitation [111]. Thus, activation of neurons closest to the electrode requires the least current. As the distance between the electrode and desired population of neurons for activation increases, larger currents are required, which generally means neurons between the electrode and desired population are also activated. Fiber diameter selectivity is the ability to activate fibers within a certain range of diameters only. Fibers with greater internodal distance and larger diameter experience greater changes in the transmembrane potential due to electrical excitation [112]. Using conventional electrical stimulation waveforms with relatively narrow pulses, the largest diameter fibers are activated at the lowest stimulus amplitude. In motor nerves, activating large-diameter fibers first corresponds to activating the largest motor units first. This recruitment order is opposite of the physiological case where the smallest motor units are recruited first. Fang and Mortimer [110] have demonstrated a waveform that allows a propagated action potential in small-diameter fibers but not large-diameter fibers. Hyperpolarizing pulses have a greater effect on larger fibers than smaller, just as for depolarizing pulses. This means that sustained hyperpolarization can be used to block action-potential initiation selectively in the large fibers, so that the corresponding depolarizing stimuli can selectively activate small fibers. Electrical-stimulation protocols have also been developed [113] for triggering of action potentials in specific cell types (e.g., interneurons) and structures (e.g., nerve terminals).

The relationship between the strength (current) of an applied constant current pulse required to initiate an action potential and the duration of the pulse, known as the strength–duration curve, is shown in Fig. 13(a). The threshold current I_{th} decreases with increasing pulse width. At very long pulse widths, the current is

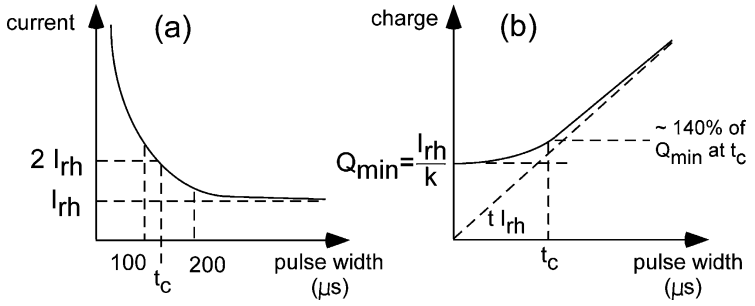

Fig. 13 Strength–Duration and Charge–Duration Curves for Initiation of an Action Potential Rheobase current I_{rh} is the current required when using an infinitely long pulse width. Chronaxie time t_c is the pulse width corresponding to two times the rheobase current

a minimum, called the rheobase current I_{rh}. The following relationship has been derived experimentally to quantify the strength–duration curve [114]:

$$I_{\mathrm{th}} = \frac{I_{\mathrm{rh}}}{1 - \exp\left(-W/\tau_{\mathrm{m}}\right)} \tag{36}$$

where I_{th} is the current required to reach threshold, I_{rh} is the rheobase current, W is the pulse width, and τ_{m} is the membrane time constant. The qualitative nature of the strength–duration curve shown is representative of typical excitable tissue. The quantitative aspects, e.g., the rheobase current, depend upon factors such as the distance between the neuron population of interest and the electrode and are determined empirically. Figure 13(b) illustrates the charge–duration curve, which plots the threshold charge $Q_{\mathrm{th}} = I_{\mathrm{th}}W$ versus pulse width. At longer pulse widths, the required charge to elicit an action potential increases due to two phenomena. First, over a period of tens to hundreds of μs, charge is redistributed through the length of the axon and does not all participate in changing the transmembrane potential at the site of injection [115, 116]. Second, over a period of several ms, accommodation (increased sodium inactivation) occurs. The minimum charge Q_{min} occurs as the pulse width approaches zero. In practice, the Q_{th} is near $Q_{\mathrm{min}}$when narrow pulses are used (tens of microseconds).

It is generally best to keep the pulse width narrow in order to minimize any electrochemical reactions occurring on the electrode surface. The narrowness of a pulse is often limited by the amount of current that can be delivered by a stimulator, especially if it is battery operated. Furthermore, some kinds of stimulation, such as selective activation of certain axons of a nerve, require pulses longer than tens of microseconds.

5 Mechanisms of Damage

An improperly designed electrical stimulation system may cause damage to the tissue being stimulated or damage to the electrode itself. Damage to an electrode can occur in the form of corrosion if the electrode is driven anodically such that the electrode potential exceeds a value where significant metal oxidation occurs. An example of such a reaction is the corrosion of platinum in a chloride-containing medium such as extracellular fluid, equation (10). Corrosion is an irreversible Faradaic process. It may be due to dissolution where the electrochemical product goes into solution or the product may form an outer solid layer on a passivation film that cannot be recovered. Charge-balanced waveforms (Fig. 9(b)) are more likely to reach potentials where corrosion may occur during the anodic-reversal phase and the open-circuit interpulse interval than are monophasic waveforms (Fig. 10). The charge-imbalanced waveform (Fig. 9(c)) has advantages both in preventing tissue damage due to sustained negative potentials during the interpulse interval, and in preventing corrosion by reducing the maximum positive potential during the anodic-reversal phase (Section 2).

The mechanisms for stimulation-induced tissue damage are not well understood. Two major classes of mechanisms have been proposed. The first is that tissue damage is caused by intrinsic biological processes as excitable tissue is overstimulated. This is called the mass-action theory and proposes that damage occurs from the induced hyperactivity of many neurons firing, or neurons firing for an extended period of time, thus changing the local environment. Proposed mass-action mechanisms include depletion of oxygen or glucose, or changes in ionic concentrations both intracellularly and extracellularly, e.g., an increase in extracellular potassium. In the CNS, excessive release of excitatory neurotransmitters such as glutamate may cause excitotoxicity. The second proposed mechanism for tissue damage is the creation of toxic electrochemical reaction products at the electrode surface during cathodic stimulation at a rate greater than that which can be tolerated by the physiological system.

McCreery et al. [117] have shown that both charge per phase and charge density are important factors in determining neuronal damage to cat cerebral cortex. In terms of the mass-action theory of damage, charge per phase determines the total volume within which neurons are excited, and the charge density determines the proportion of neurons close to an electrode that are excited; thus both factors determine the total change in the extracellular environment. The McCreery data show that as the charge per phase increases the charge density for safe stimulation decreases. When the total charge is small (as with a microelectrode) a relatively large charge density may safely be used. Tissue damage that has been attributed to mass-action effects may be alternatively explained by electrochemical means, as charge and charge density may influence the quantity of irreversible reaction products being generated at the electrode interface. Shannon [118] reprocessed the McCreery data and developed an expression for the maximum safe level for stimulation, given by

$$\log (Q/A) = k - \log (Q) \tag{37}$$

where Q is charge per phase (μC/phase), Q/A is charge density per phase ($\mu C/cm^2$/phase), and $2.0 > k > 1.5$, fit to the empirical data.

Figure 14 illustrates the charge vs. charge density relationship of equation (37) using k values of 1.7, 1.85, and 2.0, with histological data from the 1990 McCreery study using cat parietal cortex as well as data from Yuen et al. [119] on cat parietal cortex, Agnew et al. [120] on cat peroneal nerve, and Bhargava [121] on cat sacral anterior roots. Above the threshold for damage, experimental data demonstrate tissue damage, and below the threshold line, experimental data indicate no damage.

McCreery et al. [122] have reviewed damage from electrical stimulation of peripheral nerve. They concluded that damage may be from mechanical constriction of the nerve as well as neuronal hyperactivity and irreversible reactions at the electrode.

Supporting the concept that damage is due to electrochemical reaction products is the work by Lilly et al. [123], which demonstrated that loss of electrical excitability

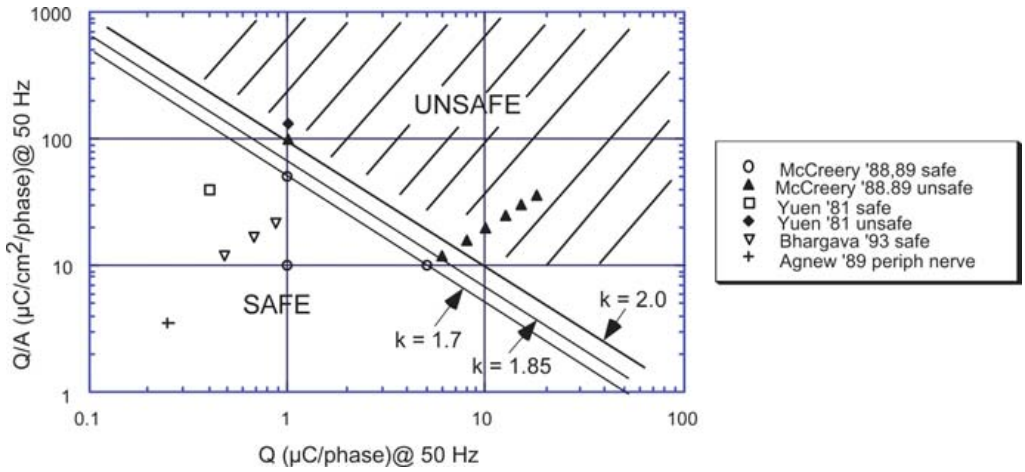

Fig. 14 Charge (Q) vs. Charge Density (Q/A) for Safe Stimulation A microelectrode with relatively small total charge per pulse might safely stimulate using a large charge density, whereas a large surface area electrode (with greater total charge per pulse) must use a lower charge density

and tissue damage occur when the cerebral cortex of monkey is stimulated using monophasic current pulses. Later, Lilly et al. [124] showed that biphasic stimulation caused no loss of excitability or tissue damage after 15 weeks of stimulation for 4–5 h per day. Lilly interpreted these results as due to movement of charged particles such as proteins out of physiological position. The concept that monophasic is a more damaging form of stimulation than charge-balanced biphasic was confirmed by Mortimer et al. [125], who reported that breakdown of the blood brain barrier during stimulation of the surface of cat cerebral cortex occurs when monophasic pulses were used at power densities greater than 0.003 W/in^2 (0.5 mW/cm^2), but does not occur with charge-balanced biphasic pulses until a power density of 0.05 W/in^2 (8 mW/cm^2) is exceeded. Pudenz et al. [126, 127] further showed that monophasic stimulation of the cat cerebral cortex causes vasoconstriction, thrombosis in venules and arterioles, and blood brain barrier breakdown within 30 s of stimulation when used at levels required for a sensorimotor response; however, charge-balanced biphasic stimulation could be used for up to 36 h continuously without tissue damage if the charge per phase was below 0.45 μC (4.5 μC/cm^2). Also supporting the hypothesis that damage is due to electrochemical products are observations of cat muscle that suggest some nonzero level of reaction product can be tolerated [88, 128]. These studies showed that monophasic stimulation causes significantly greater tissue damage than a nonstimulated implant at 1 μC/mm^2 per pulse, but not 0.2 μC/mm^2 per pulse, and that charge-balanced biphasic stimulation does not cause significant tissue damage at levels up to 2 μC/mm^2 per pulse. However, in order to prevent electrode corrosion, the charge-balanced waveform must not exceed 0.4 μC/mm^2 per pulse, otherwise the electrode potential is driven to damaging positive potentials during the anodic (reversal) phase and interpulse interval. Scheiner and Mortimer [88] studied the utility of charge-imbalanced biphasic stimulation demonstrating that this waveform allows greater cathodic charge

densities than monophasic prior to the onset of tissue damage as reactions occurring during the cathodic phase are reversed by the anodic phase, and also that greater cathodic charge densities can be used than with the charge-balanced waveform prior to electrode corrosion since the anodic phase is no longer constrained to be equal to the cathodic phase, thus the electrode potential reaches less positive values during the anodic phase and interpulse interval. Scheiner found that cat muscle tissue was significantly damaged using monophasic stimulation at 0.4 $\mu C/mm^2$ per phase, and that when charge-imbalanced biphasic stimulation was used, tissue was damaged with 1.2 $\mu C/mm^2$ per phase cathodic and 0.2 $\mu C/mm^2$ per phase anodic, and could safely tolerate 1.2 $\mu C/mm^2$ per phase cathodic and 0.5 $\mu C/mm^2$ per phase anodic. No electrode corrosion was observed under any of the conditions studied.

In 1975, Brummer and Turner [63] gave an alternative explanation to Lilly's for why biphasic pulses were less damaging than monophasic. They proposed that two principles should be followed to achieve electrochemically safe conditions during tissue stimulation:

> "(1) Perfect symmetry of the electrochemical processes in the two half-waves of the pulses should be sought. This implies that we do not generate any electrolysis products in solution. One approach to achieve this would appear to involve the use of perfectly charge-balanced waveforms of controlled magnitude. (2) The aim should be to inject charge via non-Faradaic or surface-Faradaic processes, to avoid injecting any possibly toxic materials into the body."

Their model for safe stimulation interprets the charge-balanced waveform in electrochemical terms. Any process occurring during the first (stimulating) phase, whether it is charging of the electrode or a reversible Faradaic process, is reversed during the second (reversal) phase, with no net charge delivered. The observation that monophasic stimulation causes greater tissue damage than biphasic stimulation at the same amplitude, pulse width, and frequency is explained by the fact that during monophasic stimulation, all injected charge results in generation of electrochemical reaction products.

Reversible processes include charging and discharging of the double-layer capacitance, as well as surface-bound reversible Faradaic processes such as reactions (3), (4), (5), (6), (7), (8), and (13). Reversible reactions often involve the production or consumption of hydrogen or hydroxyl ions as the charge counterion. This causes a change in the pH of the solution immediately adjacent to the electrode surface. Ballestrasse et al. [129] gave a mathematical description of these pH changes and determined that the pH may range from 4 to 10 near a 1-μm diameter electrode during biphasic current pulses, but this change extended for only a few microns. Irreversible processes include Faradaic reactions where the product does not remain near the electrode surface, such as reactions (1) and (9), (10), (11), and (12).

Free radicals are known to cause damage to myelin, the lipid cell membrane, and DNA of cells. A likely candidate for a mechanism of neural tissue damage due to electrochemical products is peroxidation of the myelin by free radicals produced on the electrode surface. Several researchers [130, 131, 132, 133, 134, 135] have demonstrated the great susceptibility of myelin to free radical damage. Damage

occurs as fatty acyl chains move apart and the myelin goes from a crystalline (ordered) state to a liquid (disordered) state.

Morton et al. [136] have shown that oxygen reduction occurs on a gold electrode in phosphate-buffered saline under typical neural stimulating conditions. Oxygen-reduction reactions that may occur during the cathodic-stimulating phase include reactions that generate free radicals such as superoxide and hydroxyl, and hydrogen peroxide, collectively known as reactive oxygen species. These species may have multiple deleterious effects on tissue [20, 21, 22, 23, 24]. As free radicals are produced, they may interfere with chemical signaling pathways that maintain proper perfusion of nervous tissue. Nitric oxide has been identified as the endothelium-derived relaxing factor, the primary vasodilator [137, 138, 139]. Nitric oxide is also known to prevent platelet aggregation and adhesion [140, 141, 142]. Beckman et al. [143] have shown that the superoxide radical reacts with nitric oxide to form the peroxynitrite radical. Oxygen-derived free radicals from the electrode may reduce the nitric oxide concentration and diminish its ability as the principal vasodilator and as an inhibitor of platelet aggregation. Superoxide depresses vascular smooth muscle relaxation by inactivating nitric oxide, as reviewed by Rubanyi [144].

An electrochemical product may accumulate to detrimental concentrations if the rate of Faradaic reaction, given by the current–overpotential relationship of equation (18), exceeds the rate for which the physiological system can tolerate the product. For most reaction products of interest there is some sufficiently low concentration near the electrode that can be tolerated over the long term. This level for a tolerable reaction may be determined by the capacity of an intrinsic buffering system. For example, changes in pH are buffered by several systems including the bicarbonate buffer system, the phosphate buffer system, and intracellular proteins. The superoxide radical, a product of the reduction of oxygen, is converted by superoxide dismutase and cytochrome c to hydrogen peroxide and oxygen. The diffusion rate of a toxic product must be considered, as it may be the case that high concentrations only exist very near the site of generation (the electrode surface).

6 Design Compromises for Efficacious and Safe Electrical Stimulation

A stimulating system must be both efficacious and safe. Efficacy of stimulation generally means the ability to elicit the desired physiological response, which can include initiation or suppression of action potentials. Safety has two primary aspects. First, the tissue being stimulated must not be damaged, and second, the stimulating electrode itself must not be damaged, as in corrosion. An electrode implanted into a human as a prosthesis may need to meet these requirements for decades. In animal experimentation, damage to the tissue or the electrode can seriously complicate or invalidate the interpretation of results.

Efficacy requires that the charge injected must exceed some threshold (Fig. 13). However, as the charge per pulse increases, the overpotential of the electrode

increases, as does the fraction of the current going into Faradaic reactions (which may be damaging to tissue or the electrode if the reaction is irreversible). Judicious design of stimulation protocols involves acceptable compromises between stimulation efficacy, requiring a sufficiently high charge per pulse, and safety, requiring a sufficiently low charge per pulse, thus preventing the electrode from reaching potentials where deleterious Faradaic reactions occur at an intolerable rate. The overpotential an electrode reaches, and thus Faradaic reactions that can occur, depend on several factors in addition to the charge per pulse, including (1) waveform type (Fig. 10), (2) stimulation frequency, (3) electrode material (a high charge-storage capacity allows relatively large charge storage prior to reaching overpotentials where irreversible Faradaic reactions occur), (4) electrode geometric area and roughness (determining real area) and therefore total capacitance, and (5) train effects (Section 2). Increasing either the stimulus phase pulse width or the reversal phase pulse width of a charge-balanced stimulation protocol has the effect of increasing unrecoverable charge into irreversible reactions. Any factor which either drives the electrode potential into a range where irreversible reactions occur (such as a long stimulus phase pulse width) or fails to quickly reverse the electrode potential out of this range (such as a long reversal phase pulse width) will allow accumulation of unrecoverable charge.

The overpotential an electrode must be driven to before any given current will be achieved is highly dependent on the kinetics of the system, characterized by the exchange current density i_0. For a system with a large exchange current density (e.g., $i_0 = 10^{-3}$ A/cm^2), no significant overpotential may be achieved before a large Faradaic current ensues (equation (18)). When i_0 is many orders of magnitude smaller (e.g., $i_0 = 10^{-9}$ A/cm^2), a large overpotential must be applied before there is substantial Faradaic current. When i_0 is very low, a large total charge can be injected through the capacitive mechanism before significant Faradaic reactions commence. This is the generally desirable paradigm for a stimulating electrode, minimizing Faradaic reactions that lead to either electrode damage or tissue damage.

The fundamental design criteria for an electrochemically safe stimulation protocol can be stated: *the electrode potential must be kept within a potential window where irreversible Faradaic reactions do not occur at levels that are intolerable to the physiological system or the electrode*. If irreversible Faradaic reactions do occur, one must ensure that they can be tolerated (e.g., that physiological buffering systems can accommodate any toxic products) or that their detrimental effects are low in magnitude (e.g., that corrosion occurs at a very slow rate, and the electrode will last for longer than its design lifetime).

The charge–duration curve shown in Fig. 13 demonstrates that to minimize the total charge injected in an efficacious stimulation protocol, one should use short-duration pulses. In practice, pulses on the order of tens of microseconds approach the minimum charge and are often reasonable design solutions. During this relatively short duration, one may be able to avoid Faradaic reactions that would occur at higher levels of total charge with longer pulses. While it is desirable to use short-duration pulses on the order of tens of microseconds, there are applications for which biological constraints require longer-duration pulses. The time constants

of several key ion channels in the membranes of excitable tissue are measured in hundreds of microseconds to milliseconds. By using stimulating pulses with comparable durations one can selectively manipulate the opening and closing of these ion channels to accomplish various specific behaviors. Certain waveforms have been developed that allow selectivity during electrical excitation of tissue (Section 4). Grill and Mortimer [145] have reviewed stimulus waveforms used for spatial and fiber diameter selective neural stimulation, illustrating the response of the neural membrane to different waveforms. Selective waveforms often require stimulation or reversal phases with long pulse widths relative to conventional stimulus waveforms; thus waveforms optimized for physiological responses may not be efficient for reversing electrochemical processes. Judicious design of electrical protocols has allowed the designers of neural prostheses to selectively inactivate the larger neurons in a nerve trunk [146], selectively inactivate the superficial fibers in a nerve by preconditioning [147], and prevent anodic break. Lastly, there are applications where tonic polarization mandates the use of very long (> 1 s) monophasic pulses; for example, tonic hyperpolarization of the soma to control epileptic activity [148, 149]. The use of these various waveforms with long pulse widths allows greater accumulation of any electrochemical product, thus requiring additional diligence by a neurophysiologist or prosthesis designer to prevent electrochemical damage.

In addition to biological constraints on the pulse durations, the required current for a short pulse width may also be a limitation. In order to inject the minimum charge required for effect, a large current is required (Fig. 13). This is not always possible, as may be the case with a battery-powered stimulator with limited current output.

Certain applications, such as clinical Deep Brain Stimulation [150, 151] and experimental long-term potentiation [152], require the use of high-frequency (> 50 Hz) pulsing. As discussed in Section 2, this can lead to a ratcheting of the electrode potential not achieved during single-pulse stimulation. Appropriate design of stimulation protocols can minimize damage by careful attention to the effects of high-frequency stimulation on the electrode potential.

Fig. 15 summarizes key features of various stimulation-waveform types. The cathodic-monophasic waveform illustrated in Fig. 15(a) consists of pulses of current passed in one direction, with an open-circuit condition during the interpulse interval. At no time does current pass in the opposite direction. Commonly the working electrode is pulsed cathodically for stimulation of tissue (as shown), although anodic stimulation may also be used (Section 4). Of the waveforms illustrated in Fig. 15, the monophasic is the most efficacious for stimulation. However, monophasic pulses are not used in long-term stimulation where tissue damage is to be avoided. Greater negative potentials are reached during monophasic pulsing than with biphasic pulsing (Fig. 10). Furthermore, the electrode potential during the interpulse interval of cathodic-monophasic pulsing remains relatively negative as the charged-electrode capacitance slowly discharges through Faradaic reactions, allowing reduction reactions which may be deleterious to tissue to proceed throughout the entire period of stimulation. Biphasic waveforms are illustrated in Fig. 15(b) to (f). The first (stimulating) phase elicits the desired physiological effect such as initiation of an

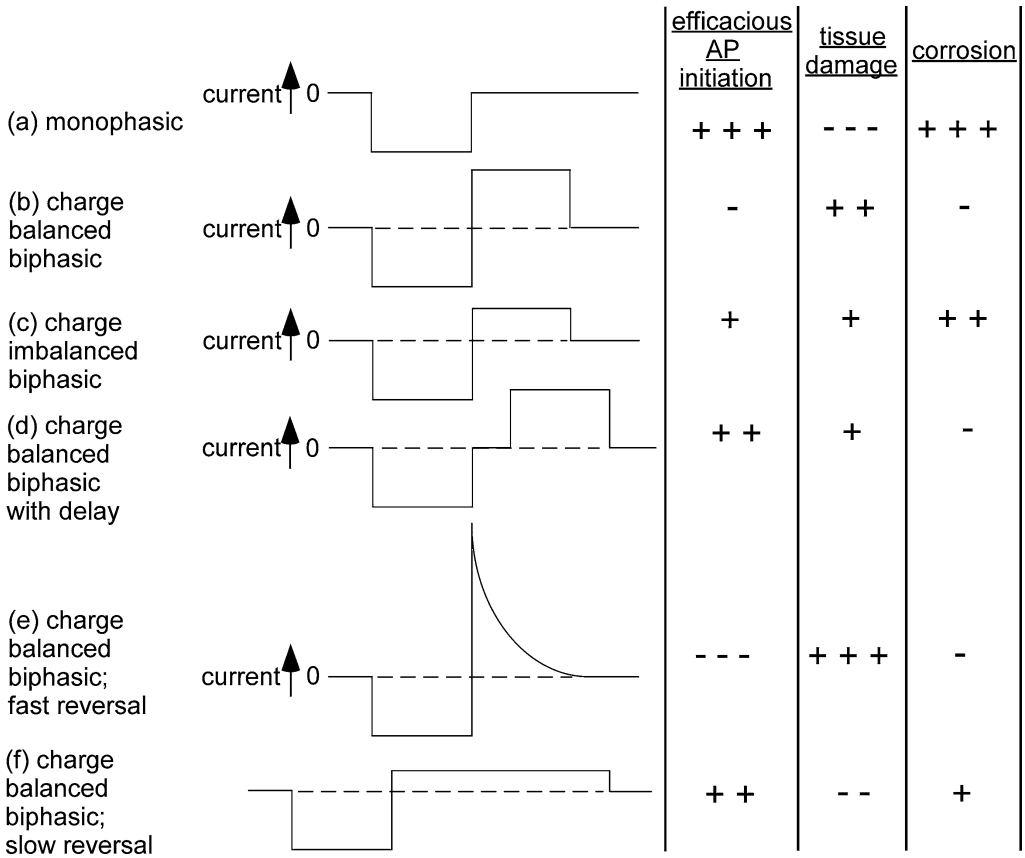

Fig. 15 Comparison of Stimulating Waveforms Six prototypical waveforms are rated for relative merit in efficacy and safety. "+++" = best (most efficacious, least damaging to tissue or the electrode), "–" = worst

action potential and the second (reversal) phase is used to reverse the direction of electrochemical processes occurring during the stimulating phase (Section 2). If all processes of charge injection during the stimulating phase are reversible, then the reversal phase will prevent net changes in the chemical environment of the electrode, as desired. The charge-balanced biphasic waveform (Fig. 15(b)) is widely used to prevent tissue damage. It should be noted that charge balance does not necessarily equate to electrochemical balance. As given by equations (32) and (33), during certain instances of stimulation there are irreversible Faradaic reactions during the cathodic phase (e.g., oxygen reduction), and then different irreversible reactions during the anodic phase (e.g., electrode corrosion) that are not the reverse of the cathodic Faradaic reactions. Such electrochemical imbalance leads to a potential waveform as illustrated in Fig. 10(b), where the potential at the end of the anodic phase is positive of the prepulse potential, allowing irreversible reactions such as electrode corrosion to occur. The charge-imbalanced waveform, illustrated in Fig. 15(c), may be used to reduce the most positive potentials during the anodic phase with respect to the charge-balanced waveform and prevent electrode corrosion [88]. Ideally, the charge in the reversal phase is equal to the charge going

into reversible processes during the stimulation phase, in which case the electrode potential returns to its prepulse value at the end of the reversal phase.

In addition to electrode corrosion, a second concern with the charge-balanced biphasic waveform is that the reversal phase not only reverses electrochemical processes of the stimulation phase, but may also reverse some of the desired physiological effect of the stimulation phase, i.e., it may suppress an action potential that would otherwise be induced by a monophasic waveform. This effect causes an increased threshold for biphasic stimulation relative to monophasic. Gorman and Mortimer [153] have shown that by introducing an open-circuit interphase delay between the stimulating and reversal phases, the threshold for biphasic stimulation is similar to that for monophasic. This is illustrated in Fig. 15(d). Although the introduction of an interphase delay improves threshold, it also allows the electrode potential to remain relatively negative during the delay period. A delay of 100 μs is typically sufficient to prevent the suppressing effect of the reversal phase, and may be a short enough period that deleterious Faradaic reaction products do not accumulate to an unacceptable level.

As illustrated in Fig. 15(e) and (f), the more rapidly charge is injected during the anodic-reversal phase, the more quickly the electrode potential is brought out of the most negative range, and thus the less likely that tissue damage will occur. A high current reversal phase however means more of a suppressing effect on action-potential initiation, and also means the electrode potential will move positive during the reversal phase, thus risking electrode corrosion.

When evaluating the electrochemistry of a stimulating electrode system, both the working electrode and counter electrode should be considered. If the area, and thus total capacitance, of a counter electrode is relatively large, there is a small potential change for a given amount of injected charge. Such an electrode will not be perturbed away from its resting potential as readily as a small electrode, and all charge injection across this large counter electrode is assumed to be by capacitive charging, not Faradaic processes. If the working electrode is driven cathodically first in a biphasic waveform (and thus the counter electrode anodically), then during the reversal phase the working electrode is driven anodically and the counter electrode cathodically. In such a system, the working electrode is often referred to simply as the cathode. Strictly speaking, the working electrode is the cathode during the stimulus phase, and during the reversal phase the roles are reversed so that the working electrode is the anode and the counter electrode is the cathode.

References

1. Merrill DR, Bikson M, Jefferys JGR (2005) Electrical stimulation of excitable tissue: design of efficacious and safe protocols. J Neurosci Methods 141(2):171–198
2. Helmholtz von HLF (1853) Ueber einige gesetze der vertheilung elektrischer strome in korperlichen leitern mit anwendung auf die thierisch-elektrischen versuche. Ann Physik 89:211–233
3. Guoy G (1910) Constitution of the electric charge at the surface of an electrolyte. J Physique 9:457–467

4. Chapman DL (1913) A contribution to the theory of electrocapillarity. Philos Mag 25: 475–481
5. Stern O (1924) Zur theorie der elektrolytischen doppelschicht. Z Elektrochem 30:508–516
6. Grahame DC (1947) The electrical double layer and the theory of electrocapillarity. Chem Rev 41:441–501
7. Randles JEB (1947) Rapid electrode reactions. Disc Faraday Soc 1:11–19
8. Gileadi E, Kirowa-Eisner E, Penciner J (1975) Interfacial Electrochemistry: An Experimental Approach. Addison-Wesley, Reading, MA, Section II
9. Bard AJ, Faulkner LR (1980) Electrochemical Methods. John Wiley and Sons, New York
10. Rand DAJ, Woods R (1974) Cyclic voltammetric studies on iridium electrodes in sulfuric acid solutions. Nature of oxygen layer and metal dissolution. J Electroanal Chem Interfacial Electrochem 55:375–381
11. Frazer EJ, Woods R (1979) The oxygen evolution reaction on cycled iridium electrodes. J Electroanal Chem 102:127–130
12. Gottesfeld S (1980) The anodic rhodium oxide film:a two-color electrochromic system. J Electrochem Soc 127:272–277
13. Dautremont-Smith WC (1982) Transition metal oxide electrochromic materials and displays: a review. Part 2. Oxides with anodic coloration. Displays 3(3):67–80
14. Delahay P (1965) Double Layer and Electrode Kinetics. Interscience Publishers, New York
15. Pletcher D, Walsh FC (1990) Industrial Electrochemistry, second edition. Chapman and Hall, London
16. Silbey RJ, Alberty RA (2001) Physical Chemistry, third edition. John Wiley and Sons, New York
17. Ives DJG, Janz GJ (1961) Reference Electrodes: Theory and Practice. Academic Press, New York
18. Rand DAJ, Woods R (1971) The nature of adsorbed oxygen on rhodium, palladium, and gold electrodes. J Electroanal Chem Interfacial Electrochem 31:29–38
19. Michael DJ, Wightman RM (1999) Electrochemical monitoring of biogenic amine neurotransmission in real time. J Pharm Biomed Anal 19:33–46
20. Halliwell B (1992) Reactive oxygen species and the central nervous system. J Neurochem 59(5):1609–1623
21. Stohs SJ (1995) The role of free radicals in toxicity and disease. J Basic Clin Physiol Pharmacol 6(3–4):205–228
22. Hemnani T, Parihar MS (1998) Reactive oxygen species and oxidative DNA damage. Indian J Physiol Pharmacol 42(4):440–452
23. Imlay JA (2003) Pathways of oxidative damage. Annu Rev Microbiol 57:395–418
24. Bergamini CM, Gambetti S, Dondi A, Cervellati C (2004) Oxygen, reactive oxygen species and tissue damage. Curr Pharm Des 10(14):1611–1626
25. Donaldson NdN, Donaldson PEK (1986) When are actively balanced biphasic ('Lilly') stimulating pulses necessary in a neural prosthesis? I.Historical background, Pt resting potential, dQ studies. Med and Biol Eng and Comput 24:41–49
26. Donaldson NdN, Donaldson PEK (1986) When are actively balanced biphasic ('Lilly') stimulating pulses necessary in a neural prosthesis? II.pH changes, noxious products, electrode corrosion, discussion. Med and Biol Eng and Comput 24:50–56
27. Weinman J, Mahler J (1964) An analysis of electrical properties of metal electrodes. Med Electron Biol Eng 2:229–310
28. Dymond AM, Kaechele LE, Jurist JM, Crandall PH (1970) Brain tissue reaction to some chronically implanted metals. J Neurosurg 33:574–580
29. Stensaas SS, Stensaas LJ (1978) Histopathological evaluation of materials implanted in the cerebral cortex. Acta Neuropathol 41:145–155
30. Loeb GE, Walker AE, Vematsu S, Konigsmark BW (1977) Histological reaction to various conductive and dielectric films chronically implanted in the subdural space. J Biomed Mater Res 11(2):195–210

31. Majji AB, Humayun MS, Weiland JD, Suzuki S, D'Anna SA, deJuan E Jr (1999) Long-term histological and electrophysiological results of an inactive epiretinal electrode array implantation in dogs. Invest Opthalmol Vis Sci 40(9):2073–2081
32. Chouard CH, Pialoux P (1995) Biocompatibility of cochlear implants. Bull Acad Natl Med 179(3):549–555
33. Niparko JK, Altschuler RA, Xue XL, Wiler JA, Anderson DJ (1989) Surgical implantation and biocompatibility of central nervous system auditory prostheses. Ann Otol Rhinol Laryngol 98(12 Pt 1):965–970
34. Babb TL, Kupfer W (1984) Phagocytic and metabolic reactions to chronically implanted metal brain electrodes. Exp Neurol 86(2):171–182
35. Fisher G, Sayre GP, Bickford RC (1961) Histological changes in the cat's brain after introduction of metallic and plastic-coated wire. In: Sheer DE (ed) Electrical Stimulation of the Brain. Univ. of Texas Press, Austin, 55–59
36. Sawyer PN, Srinivasan S (1974) In Ray CD (ed) Medical Engineering. Chicago 1099–1110.
37. Ryhanen J, Kallioinen M, Tuukkanen J, Junila J, Niemela E, Sandvik P, Serlo W (1998) In vivo biocompatibility evaluation of nickel-titanium shape memory alloy: muscle and perineural tissue responses and encapsule membrane thickness. J Biomed Mater Res 41(3):481–488
38. Bogdanski D, Koller M, Muller D, Muhr G, Bram M, Buchkremer HP, Stover D, Choi J, Epple M (2002) Easy assessment of the biocompatibility of Ni-Ti alloys by in vitro cell culture experiments on a functionally graded Ni-NiTi-Ti material. Biomaterials 22(23):4549–4555
39. Jones KE, Campbell PK, Normann RA (1992) A glass/silicon composite intracortical electrode array. Ann Biomed Eng 20(4):423–437
40. Hoogerwerf AC, Wise KD (1994) A three-dimensional microelectrode array for chronic neural recording. IEEE Trans Biomed Eng 41:1136–1146
41. Rousche PJ, Pellinen DS, Pivin DP, Williams JC, Vetter RJ, Kipke DR (2001) Flexible polyimide-based intracortical electrode arrays with bioactive capability. IEEE Trans Biomed Eng 48(1):361–370
42. Kennedy PR (1989) The cone electrode:A long-term electrode that records from neurites grown onto its recording surface. J Neurosci Methods 29(3):181–193
43. Kennedy PR, Bakay RA (1998) Restoration of neural output from a paralyzed patient by a direct brain connection. Neuroreport 9(8):1707–1711
44. Kennedy PR, Bakay RA, Moore M, Adams K, Montgomery G (1999) Neural activity during acquisition of cursor control in a locked-in patient. Soc Neurosci Abstr 25(1):894
45. Rudge JS, Smith GM, Silver J (1989) An in vitro model of wound healing in the central nervous system: analysis of cell reaction and interaction at different times. Exp Neurol 103:1–16
46. Turner JN, Shain W, Szarowski DH, Andersen M, Martins S, Isaacson M, Craighead H (1999) Cerebral astrocyte response to micromachined silicon implants. Exp Neurol 156: 33–49
47. Bignami A, Dahl D (1976) The astroglial response to stabbing: immunoflourescence studies with antibodies to astrocyte-specific protein (GFA) in mammalian and sub-mammalian vertebrate. Neuropathol Appl Neurobiol 251:23–43
48. Robblee LS, Rose TL (1990) Electrochemical guidelines for selection of protocols and electrode materials for neural stimulation. In: Agnew WF, McCreery DB (ed) Neural Prostheses: Fundamental Studies. Prentice-Hall, Englewood Cliffs 25–66.
49. Merrill DR (2002) Electrochemical processes occurring on gold in sulfuric acid under neural stimulation conditions, Ph.D. thesis, Case Western Reserve University, Dept. of Biomedical Engineering, Cleveland,OH
50. Merrill DR, Stefan IC, Scherson DA, Mortimer JT (2005) Electrochemistry of gold in aqueous sulfuric acid solutions under neural stimulation conditions. J Electrochem Soc 152(7):E212–E221

51. White RL, Gross TJ (1974) An evaluation of the resistance to electrolysis of metals for use in biostimulation probes. IEEE Trans Biomed Eng BME-21:487–490
52. Johnson PF, Hench LL (1977) An in vitro analysis of metal electrodes for use in the neural environment. Brain Behav Evol 14:23–45
53. Brummer SB, McHardy J, Turner MJ (1977) Electrical stimulation with Pt electrodes: Trace analysis for dissolved platinum and other dissolved electrochemical products. Brain Behav Evol 14:10–22
54. Black RD, Hannaker P (1979) Dissolution of smooth platinum electrodes in biological fluids. Appl Neurophysiol 42:366–374
55. McHardy J, Robblee RS, Marsten M, Brummer SB (1980) Electrical stimulation with platinum electrodes. IV. Factors influencing platinum dissolution in inorganic saline. Biomater B1:129–134
56. Robblee RS, McHardy J, Marsten M, Brummer SB (1980) Electrical stimulation with platinum electrodes. V. The effects of protein on platinum dissolution. Biomater B1:135–139
57. Robblee RS, Lefko JL, Brummer SB (1983) Activated iridium: An electrode suitable for reversible charge injection in saline solution. J Electrochem Soc 130:731–733
58. Robblee RS, McHardy J, Agnew WF, Bullara LA (1983) Electrical stimulation with Pt electrodes. VII. Dissolution of Pt electrodes during electrical stimulation of the cat cerebral cortex. J Neurosci Methods 9:301–308
59. Tivol WF, Agnew WF, Alvarez RB, Yuen TGH (1987) Characterization of electrode dissolution products on the high voltage electrode microscope. J Neurosci Methods 19:323–337
60. Rosenberg B, VanCamp L, Krigas T (1965) Inhibition of cell division in Escherichia coli by electrolysis products from a platinum electrode. Nature 205:698–699
61. Rosenberg B (1971) Some biological effects of platinum compounds: New agents for the control of tumours. Platin Met Rev 15:42–51
62. Macquet JP, Theophanides T (1976) DNA-Platinum interactions. Characterization of solid DNA-$K_2[PtCl_4]$ complexes. Inorg Chim Acta 18:189–194
63. Brummer SB, Turner MJ (1975) Electrical stimulation of the nervous system: the principle of safe charge injection with noble metal electrodes. Bioelectrochem Bioenerg 2:13–25
64. Brummer SB, Turner MJ (1977) Electrochemical considerations for safe electrical stimulation of the nervous system with platinum electrodes. IEEE Trans Biomed Eng BME-24: 59–63
65. Brummer SB, Turner MJ (1977) Electrical stimulation with Pt electrodes. I. A method for determination of 'real' electrode areas. IEEE Trans Biomed Eng BME-24:436–439
66. Brummer SB, Turner MJ (1977) Electrical stimulation with Pt electrodes. II. Estimation of maximum surface redox (theoretical non-gassing) limits. IEEE Trans Biomed Eng BME-24:440–443
67. Rose TL, Robblee LS (1990) Electrical stimulation with Pt electrodes. VIII. Electrochemically safe charge injection limits with 0.2 ms pulses. IEEE Trans Biomed Eng 37(11):1118–1120
68. Bruckenstein S, Miller B (1970) An experimental study of non-uniform current distribution at rotating disk electrodes. J Electrochem Soc 117:1044–1048
69. Shepherd RK, Murray MT, Houghton ME, Clark GM (1985) Scanning electron microscopy of chronically stimulated platinum intracochlear electrodes. Biomater 6:237–242
70. Wiley JD, Webster JJ (1982) Analysis and control of the current distribution under circular dispersive electrodes. IEEE Trans Biomed Eng BME-29:381–385
71. Zerbino JO, Tacconi NR, Arvia AJ (1978) The activation and deactivation of iridium in acid electrolytes. J Electrochem Soc 125:1266–1276
72. Mozota J, Conway BE (1983) Surface and bulk processes at oxidized iridium electrodes-I: monolayer stage and transition to reversible multilayer oxide film behavior. Electrochimica Acta 28:1–8
73. Bak MK, Girvin JP, Hambrecht FT, Kufta CV, Loeb GE, Schmidt EM (1990) Visual sensations produced by intracortical microstimulation of the human occipital cortex. Med Biol Eng Comput 28:257–259

74. McCreery DB, Yuen TGH, Agnew WF, Bullara LA (1992) Stimulation with chronically implanted microelectrodes in the cochlear nucleus of the cat: histologic and physiologic effects. Hear Res 62:42–56
75. Loeb GE, Peck RA, Martyniuk J (1995) Toward the ultimate metal microelectrode. J Neurosci Methods 63:175–183
76. Liu X, McCreery DB, Carter RR, Bullara LA, Yuen TGH, Agnew WF (1999) Stability of the interface between neural tissue and chronically implanted intracortical microelectrodes. IEEE Trans Rehabil Eng 7(3):315–326
77. Meyer RD, Cogan SF (2001) Electrodeposited iridium oxide for neural stimulation and recording electrodes. IEEE Trans Neural Syst Rehabil Eng 9(1):2–10
78. Anderson DJ, Najafi K, Tanghe SJ, Evans DA, Levy KL, Hetke JF, Xue X, Zappia JJ, Wise KD (1989) Batch-fabricated thin-film electrodes for stimulation of the central auditory system. IEEE Trans Biomed Eng 36:693–704
79. Weiland JD, Anderson DJ (2000) Chronic neural stimulation with thin-film, iridium oxide electrodes. IEEE Trans Biomed Eng 47(7):911–918
80. Beebe X, Rose TL (1988) Charge injection limits of activated iridium oxide electrodes with 0.2 ms pulses in bicarbonate buffered saline. IEEE Trans Biomed Eng BME-35:494–495
81. Kelliher EM, Rose TL (1989) Evaluation of charge injection properties of thin film redox materials for use as neural stimulation electrodes. Mater Res Soc Symp Proc 110:23–27
82. Agnew WF, Yuen TGH, McCreery DB, Bullara LA (1986) Histopathologic evaluation of prolonged intracortical electrical stimulation. Exp Neurol 92:162–185
83. Robblee LS, Mangaudis MM, Lasinsky ED, Kimball AG, Brummer SB (1986) Charge injection properties of thermally-prepared iridium oxide films. Mater Res Soc Symp Proc 55:303–310
84. Klein JD, Clauson SL, Cogan SF (1989) Morphology and charge capacity of sputtered iridium oxide films. J Vac Sci Technol A7:3043–3047
85. Loucks RB, Weinberg H, Smith M (1959) The erosion of electrodes by small currents. Electroenceph Clin Neurophysiol 11:823–826
86. Greatbatch W, Chardack WM (1968) Myocardial and endocardiac electrodes for chronic implantation. Ann N.Y Acad Sci 148:234–251
87. McHardy J, Geller D, Brummer SB (1977) An approach to corrosion control during electrical stimulation. Ann Biomed Eng 5:144–149
88. Scheiner A, Mortimer JT (1990) Imbalanced biphasic electrical stimulation: muscle tissue damage. Ann Biomed Eng 18:407–425
89. Gotman I (1997) Characteristics of metals used in implants. J Endourol 11(6):383–389
90. Guyton DL, Hambrecht FT (1973) Capacitor electrode stimulates nerve or muscle without oxidation-reduction reactions. Science 181:74–76
91. Guyton DL, Hambrecht FT (1974) Theory and design of capacitor electrodes for chronic stimulation. Med and Biol Eng 7:613–620
92. Rose TL, Kelliher EM, Robblee LS (1985) Assessment of capacitor electrodes for intracortical neural stimulation. J Neurosci Methods 12(3):181–193
93. Johnson PF, Bernstein JJ, Hunter G, Dawson WW, Hench LL (1977) An in vitro and in vivo analysis of anodized tantalum capacitive electrodes: corrosion response, physiology and histology. J Biomed Mater Res 11:637–656
94. McCreery DB, Bullara LA, Agnew WF (1986) Neuronal activity evoked by chronically implanted intracortical microelectrodes. Exp Neurol 92:147–161
95. Hille B (1984) Ionic Channels of Excitable Membranes. Sinauer Associates, Sunderland, MA
96. Kandel ER, Schwartz JH, Jessell TM (2000) Principles of Neural Science, fourth ed. McGraw Hill, New York
97. Chiu SY, Ritchie JM, Rogart RB, Stagg D (1979) A quantitative description of membrane current in rabbit myelinated nerve. J Physiol 292:149–166
98. Sweeney JD, Durand D, Mortimer JT (1987) Modeling of mammalian myelinated nerve for functional neuromuscular stimulation. Proc. 9th Intl. Conf. IEEE-EMBS, 1577–1578

99. Hodgkin AL, Huxley AF (1952) Currents carried by sodium and potassium ions through the membrane of the giant axon of Loligo. J Physiol 116:449–472
100. Hodgkin AL, Huxley AF (1952) The Components of membrane conductance in the giant axon of logigo. J Physiol 116:473–496
101. Hodgkin AL, Huxley AF (1952) The dual effect of membrane potential on sodium conductance in the giant axon of logigo. J Physiol 116:497–506
102. Hodgkin AL, Huxley AF (1952) A quantitative description of the membrane current and its application to conduction and excitation in nerve. J Physiol 117:500–544
103. McNeal DR (1976) Analysis of a model for excitation of myelinated nerve. IEEE Trans Biomed Eng 23(4):329–337
104. Ranck JB (1981) In: Patterson MM, Kesner RP (ed) Electrical Stimulation Research Techniques. Academic Press, New York, chapter 1
105. Mortimer JT (1990) In: Agnew WF, McCreery DB (ed) Neural Prostheses: Fundamental Studies. Prentice-Hall. Englewood Cliffs, chapter 3.
106. Durand D (1995) In: Bronzino JD (ed) Biomedical Engineering Handbook. CRC Press, Boca Raton, chapter 17
107. van den Honert C, Mortimer JT (1979) Generation of unidirectionally propagated action potentials in a peripheral nerve by brief stimuli. Science 206(4424):1311–1312
108. van den Honert C, Mortimer JT (1981) A technique for collision block of peripheral nerve: single stimulus analysis. IEEE Trans Biomed Eng 28:373–378
109. van den Honert C, Mortimer JT (1981) A technique for collision block of peripheral nerve: frequency dependence. IEEE Trans Biomed Eng 28:379–382
110. Fang Z, Mortimer JT (1991) Selective activation of small motor axons by quasitrapezoidal current pulses. IEEE Trans Biomed Eng 38(2):168–174
111. Rall W (1977) In: Handbook of Physiology-The Nervous System I, vol.1/Part 1. American Physiological Society, chapter 3.
112. Rattay F (1989) Analysis of models for extracellular fiber stimulation. IEEE Trans Biomed Eng 36:676–682
113. McIntyre CC, Grill WM (2002) Extracellular stimulation of central neurons: influence of stimulus waveform and frequency on neuronal output. J Neurophysiol 88(4):1592–1604
114. Lapicque L (1907) Recherches quantitatives sur l'excitation electrique des nerfs traites comme une polarization. J Physiol (Paris) 9:622–635
115. Warman EN, Grill WM, Durand D (1992) Modeling the effects of electric fields on nerve fibers: determination of excitation thresholds. IEEE Trans Biomed Eng 39(12):1244–1254
116. Plonsey R, Barr RC (1988) Bioelectricity: A Quantitative Approach. Plenum press, New York
117. McCreery DB, Agnew WF, Yuen TGH, Bullara LA (1990) Charge density and charge per phase as cofactors in neural injury induced by electrical stimulation. IEEE Trans Biomed Eng 37(10):996–1001
118. Shannon RV (1992) A model of safe levels for electrical stimulation. IEEE Trans Biomed Eng 39(4):424–426
119. Yuen TGH, Agnew WF, Bullara LA, Jacques S, McCreery DB (1981) Histological evaluation of neural damage from electrical stimulation: considerations for the selection of parameters for clinical application. Neurosurg 9(3):292–299
120. Agnew WF, McCreery DB, Yuen TGH, Bullara LA (1989) Histologic and physiologic evaluation of electrically stimulated peripheral nerve: considerations for the selection of parameters. Ann Biomed Eng 17:39–60
121. Bhargava A (1993) Long-term effects of quasi-trapezoidal pulses on the structure and function of sacral anterior roots. M.S. thesis, Case Western Reserve University, Dept. of Biomedical Engineering, Cleveland, OH
122. McCreery DB, Agnew WF, Yuen TGH, Bullara LA (1992) Damage in peripheral nerve from continuous electrical stimulation: comparison of two stimulus waveforms. Med Biol Eng Comput 30(1):109–114

123. Lilly JC, Austin GM, Chambers WW (1952) Threshold movements produced by excitation of cerebral cortex and efferent fibers with some parametric regions of rectangular current pulses (cats and monkeys). J Neurophysiol 15:319–341
124. Lilly JC, Hughes JR, Alvord EC, Garkin TW (1955) Brief noninjurious electric waveforms for stimulation of the brain. Science 121:468–469
125. Mortimer JT, Shealy CN, Wheeler C (1970) Experimental nondestructive electrical stimulation of the brain and spinal cord. J Neurosurg 32(5):553–559
126. Pudenz RH, Bullara LA, Dru D, Talalla A (1975) Electrical stimulation of the brain II: effects on the blood-brain barrier. Surg Neurol 4:265–270
127. Pudenz RH, Bullara LA, Jacques P, Hambrecht FT (1975) Electrical stimulation of the brain III: the neural damage model. Surg Neurol 4:389–400
128. Mortimer JT, Kaufman D, Roessmann U (1980) Intramuscular electrical stimulation: tissue damage. Ann Biomed Eng 8:235–244
129. Ballestrasse CL, Ruggeri RT, Beck TR (1985) Calculations of the pH changes produced in body tissue by a spherical stimulation electrode. Ann Biomed Eng 13:405–424
130. Chan PH, Yurko M, Fishman R (1982) Phospholipid degradation and cellular edema induced by free radicals in brain slice cortical slices. J Neurochem 38:525–531
131. Chia LS, Thompson JE, Moscarello MA (1983) Disorder in human myelin induced by superoxide radical: an in vitro investigation. Biochem and Biophys Res Commun 117(1):141–146
132. Konat G, Wiggins RC (1985) Effect of reactive oxygen species on myelin membrane proteins. J Neurochem 45:1113–1118
133. Sevanian A (1988) In: Lipid Peroxidation, Membrane Damage, and Phospholipase A2 Action. CRC Reviews, Cellular Antioxidant Defense Mechanisms, Vol.II, 77–95
134. Griot C, Vandevelde RA, Peterhans E, Stocker R (1990) Selective Degeneration of oligiodendrocytes mediated by reactive oxygen species. Free Radic Res Commun 11(4,5):181–193
135. Buettner GR (1993) The pecking order of free radicals and antioxidants: lipid peroxidation, alpha-tocopherol, and ascorbate. Arch Biochem Biophys 300(2):535–543
136. Morton SL, Daroux ML, Mortimer JT (1994) The role of oxygen reduction in electrical stimulation of neural tissue. J Electrochem Soc 141:122–130
137. Furchgott RF (1988) Studies on relaxation of rabbit aorta by sodium nitrite: the basis for the proposal that the acid-activatable inhibitory factor from retractor penis is inorganic nitrite and the endothelium-derived relaxing factor is nitric oxide, vasodilatation. In: Vascular Smooth Muscle, Peptides, Autonomic Nerves and Endothelium. Raven Press, New York, 401–414
138. Ignarro LJ, Byrns RE, Wood KS (1988) Biochemical and pharmacological properties of endothelium-derived relaxing factor and its similarity to nitric oxide radical. In: Vascular Smooth Muscle, Peptides, Autonomic Nerves and Endothelium. Raven Press, New York, 427–436
139. Umans J, Levi R (1995) Nitric oxide in the regulation of blood flow and arterial pressure. Ann Rev Physiol 57:771–790
140. Azuma H, Ishikawa M, Sekizaki S (1986) Endothelium-dependent Inhibition of Platelet Aggregation. British J Pharm 88:411–415
141. Radomski MW, Palmer RMJ, Moncada S (1987) Endogenous nitric oxide inhibits human platelet adhesion to vascular endothelium. Lancet 2:1057–1058
142. Moncada S, Palmer RMJ, Higgs EA (1991) Nitric oxide: Physiology, Pathology and Pharmacology. Pharmacol Rev 43(2):109–142
143. Beckman JS, Beckman TW, Chen J, Marshall PA, Freeman BA (1990) Apparent hydroxyl radical production by peroxynitrite: implications for endothelial injury from nitric oxide and superoxide. Proc Natl Acad Sci USA 87:1620–1624
144. Rubanyi GM (1988) Vascular Effects of Oxygen Derived Free Radicals. Free Radic Biol and Med 4:107–120
145. Grill WM, Mortimer JT (1995) Stimulus waveforms for selective neural stimulation. IEEE Eng Med Biol 14:375–385

146. Fang Z, Mortimer JT (1991) A method to effect physiological recruitment order in electrically activated muscle. IEEE Trans Biomed Eng 38(2):175–179
147. Grill WM, Mortimer JT (1997) Inversion of the current-distance relationship by transient depolarization. IEEE Trans Biomed Eng 44 (1):001–009
148. Gluckman BJ, Neel EJ, Netoff TI, Ditto WL, Spano ML, Schiff SJ (1996) Electric field suppression of epileptiform activity in hippocampal slices. J Neurophysiol 76(6):4202–4205
149. Ghai RS, Bikson M, Durand DM (2000) Effects of applied electric fields on low-calcium epileptiform activity in the CA1 region of rat hippocampal slices. J Neurophysiol 84(1): 274–280
150. McIntyre CC, Thakor NV (2002) Uncovering the mechanisms of deep brain stimulation for Parkinson's disease though functional imaging, neural recording, and neural modeling. Crit Rev Biomed Eng 30(4–6):249–281
151. O'Suilleabhain PE, Frawley W, Giller C, Dewey RB (2003) Tremor response to polarity, voltage, pulsewidth and frequency of thalamic stimulation. Neurology 60(5):786–790
152. Bliss TV, Lomo T (1973) Long-lasting potentiation of synaptic transmission in the dentate area of the anaesthetized rabbit following stimulation of the perforant path. J Physiol 232(2):331–356
153. Gorman PH, Mortimer JT (1983) The effect of stimulus parameters on the recruitment characteristics of direct nerve stimulation. IEEE Trans Biomed Eng BME-30:407–414
154. Stieglitz T, Meyer JU (1999) Implantable microsystems. Polyimide-based neuroprostheses for interfacing nerves. Med Dev Technol 10(6):28–30
155. Schmidt S, Horch K, Normann R (1993) Biocompatibility of silicon-based electrode arrays implanted into feline cortical tissue. J Biomed Mater Res 27(11):1393–1399
156. Kristensen BW, Noraberg J, Thiebaud P, Koudelka-Hep M, Zimmer J (2001) Biocompatibility of silicon-based arrays of electrodes coupled to organotypic hippocampal brain slice cultures. Brain Res 896:1–17
157. Bernstein JJ, Hench LL, Johnson PF, Dawson WW, Hunter G (1977) Electrical stimulation of the cortex with Ta_2O_5 capacitive electrodes. In: Hambrecht FT, Reswick JB (ed) Functional Electrical Stimulation. Marcel-Dekker, New York, 465–477
158. Donaldson PEK (1974) The stability of tantalum-pentoxide films in vivo. Med Biol Eng 12:131–135
159. Lagow CH, Sladek KJ, Richardson PC (1971) Anodic insulated tantalum oxide electrocardiograph electrodes. IEEE Trans Biomed Eng 18:162–164